RADC-TR-88-227
Final Technical Report
October 1988

AUTONOMOUS NAVIGATION AND CONTROL

MICROCOSM, Inc.

Sponsored by
Defense Advanced Research Projects Agency
ARPA Order No. 9132

APPROVED FOR PUBLIC RELEASE; DISTRIBUTION UNLIMITED.

ROME AIR DEVELOPMENT CENTER
Air Force Systems Command
Griffiss Air Force Base, NY 13441-5700

This report has been reviewed by the RADC Public Affairs Division (PA) and is releasable to the National Technical Information Service (NTIS). At NTIS it will be releasable to the general public, including foreign nations.

RADC-TR-88-227 has been reviewed and is approved for publication.

APPROVED: Steven W. Kabelis, 1Lt, USAF

STEVEN W. KABELIS, 1Lt, USAF
Project Engineer

APPROVED: Francis G. Reid

FRANCIS G. REID, Colonel, USAF
Acting Director of Communications

FOR THE COMMANDER: James W. Hyde III

JAMES W. HYDE III
Directorate of Plans & Programs

If your address has changed or if you wish to be removed from the RADC mailing list, or if the addressee is no longer employed by your organization, please notify RADC (DCCR) Griffiss AFB NY 13441-5700. This will assist us in maintaining a current mailing list.

Do not return copies of this report unless contractual obligations or notices on a specific doucment require that it be returned.

AUTONOMOUS NAVIGATION AND CONTROL

Peter D. Noerdlinger
Frank M. Tai

Contractor: MICROCOSM, Inc.
Contract Number: F30602-87-C-0056
Program Code Number: 7223
Effective Date of Contract: 7 June 1987
Contract Expiration Date: 7 June 1988
Short Title of Work: Autonomous Navigation and Control
Period of Work Covered: Jun 87 - Jun 88

Principal Investigator: Peter D. Noerdlinger
Phone: (213) 539-9444

RADC Project Engineer: Steven W. Kabelis, 1Lt, USAF
Phone: (315) 330-3091

This research was supported by the Defense Advanced Research Projects Agency of the Department of Defense and was monitored by Steven W. Kabelis, 1Lt, USAF, RADC (DCCR) Griffiss AFB NY 13441-5700 under Contract F30602-87-C-0056.

UNCLASSIFIED

SECURITY CLASSIFICATION OF THIS PAGE

REPORT DOCUMENTATION PAGE

Form Approved OMB No. 0704-0188

1a. REPORT SECURITY CLASSIFICATION UNCLASSIFIED	1b. RESTRICTIVE MARKINGS N/A
2a. SECURITY CLASSIFICATION AUTHORITY N/A	3. DISTRIBUTION/AVAILABILITY OF REPORT Approved for public release; distribution unlimited.
2b. DECLASSIFICATION/DOWNGRADING SCHEDULE N/A	
4. PERFORMING ORGANIZATION REPORT NUMBER(S) 880601	5. MONITORING ORGANIZATION REPORT NUMBER(S) RADC-TR-88-227
6a. NAME OF PERFORMING ORGANIZATION MICROCOSM, Inc. — 6b. OFFICE SYMBOL (If applicable)	7a. NAME OF MONITORING ORGANIZATION Rome Air Development Center (DCCR)
6c. ADDRESS (City, State, and ZIP Code) Rolling Hills Office Plaza 2601 Airport Drive, Suite 230 Torrance CA 90505	7b. ADDRESS (City, State, and ZIP Code) Griffiss AFB NY 13441-5700
8a. NAME OF FUNDING/SPONSORING ORGANIZATION Defense Advanced Research Projects Agency — 8b. OFFICE SYMBOL (If applicable) ISTO	9. PROCUREMENT INSTRUMENT IDENTIFICATION NUMBER F30602-87-C-0056
8c. ADDRESS (City, State, and ZIP Code) 1400 Wilson Blvd Arlington VA 22209	10. SOURCE OF FUNDING NUMBERS

PROGRAM ELEMENT NO.	PROJECT NO.	TASK NO	WORK UNIT ACCESSION NO.
63223C	I132	00	02

11. TITLE (Include Security Classification)
AUTONOMOUS NAVIGATION AND CONTROL

12. PERSONAL AUTHOR(S)
Peter D. Noerdlinger, Frank M. Tai

13a. TYPE OF REPORT	13b. TIME COVERED	14. DATE OF REPORT (Year, Month, Day)	15. PAGE COUNT
Final	FROM Jun 87 TO Jun 88	October 1988	80

16. SUPPLEMENTARY NOTATION
N/A

17. COSATI CODES			18. SUBJECT TERMS (Continue on reverse if necessary and identify by block number)
FIELD	GROUP	SUB-GROUP	Spacecraft Navigation Control
17	07		

19. ABSTRACT (Continue on reverse if necessary and identify by block number)

This study provided a detailed analysis of the capabilities and limitations of a single, on-board satellite sensor and processor in providing simultaneous determination of spacecraft position and attitude without the need for ground telemetry or dependence on the Global Positioning System (GPS). Hardware design, including size and weight, along with software performance measurements and testing data is included in the effort.

20. DISTRIBUTION/AVAILABILITY OF ABSTRACT	21. ABSTRACT SECURITY CLASSIFICATION
☒ UNCLASSIFIED/UNLIMITED ☐ SAME AS RPT ☐ DTIC USERS	UNCLASSIFIED

22a. NAME OF RESPONSIBLE INDIVIDUAL	22b TELEPHONE (Include Area Code)	22c. OFFICE SYMBOL
Steven W. Kabelis, 1Lt, USAF	(315) 330-3091	RADC (DCCR)

DD Form 1473, JUN 86 — Previous editions are obsolete. — SECURITY CLASSIFICATION OF THIS PAGE

UNCLASSIFIED

Table of Contents

List of Figures

List of Tables

ABSTRACT

The Autonomous Navigation System (ANS) is capable of achieving positioning accuracies of 100 m. to 1.5 km. with straightforward modifications to existing Earth sensing hardware. Because it uses hardware that would be on board the spacecraft for attitude determination, the additional cost for achieving fully autonomous navigation will be quite low. The modifications will allow the sensor to measure the size of the Earth and sense the relative positions in the spacecraft sky of the Earth, Moon, and Sun. Because the measurements can be made with a single sensor, including independent redundant observations, many of the principal bias terms can be eliminated or greatly reduced.

Additional work is needed to fully develop the cost versus performance of the autonomous navigation model. No new technology is required, although some calibration or bias determination techniques may need to be developed to accommodate the evolving sensor accuracy. The proposed system could have a significant impact on ground operations costs, mission definition and design, survivability, and the potential development of very low cost fully autonomous spacecraft.

1. Introduction

The Multiple Satellite System Program (MSSP) was jointly sponsored by DARPA and Rome Air Development Center (RADC) to develop a low cost, highly survivable communication system. Its preliminary design phase was concluded in early 1987 with contributions from Ball Aerospace, Cincinnati Electronics, COMSAT, DSI, Harris Corporation, M/A-COM, Qualcomm, RCA, Rockwell and SPACECOM. The objective of the satellite constellation was to provide global prioritized data-voice service during peacetime and essential communications during crises. This was to be accomplished by emphasizing satellite survivability and constellation flexibility during the design. One of the goals which evolved from the survivability objective was the need for autonomous operation, i.e., that the satellites not be dependent on any ground node or other satellite. This goal led to this study on low cost satellite autonomous navigation.

2. Conceptual Basis of Autonomous Navigation Approach

2.1. Satellite Autonomous Navigation History

Navigation is the ability to determine one's position and velocity. Autonomous navigation is the ability to perform this function onboard in real time and independently of external sources.

Autonomous satellite navigation has been of interest since the beginning of space flight. Flight applications began as early as 1963. Various complements of sensors have been used including horizon scanners, known landmark trackers, unknown landmark trackers, star sensors, strapdown gyros, mosaic sensors, and space sextants. Table 1, from Reference 1, traces the history of satellite autonomous navigation development.

Recent activities in the development of autonomous satellite navigation have emphasized four general methods: 1) direct Earth horizon sensing, 2) inferred Earth horizon sensing through stellar refraction, 3) satellite crosslinks, and 4) use of Navstar or the Global Positioning System (GPS). Fig. 1, also from Reference 1, represents actual and projected position accuracies using these methods.

Method 2 requires the use of onboard star sensors, method 3 requires the instrumentation necessary to make satellite-to-satellite ranging measurements, and method 4 is not fully autonomous as it requires ground-based monitor stations and updates from the GPS satellites. Only method 1 remains as a means for providing truly low cost and autonomous satellite navigation.

2.2 Earth, Sun and Moon Autonomous Navigation

The concept behind the current low cost autonomous navigation system is to determine the satellite position based on the directions to the Earth, Sun and Moon and the distance to the Earth, as illustrated in Figure 2. This can be accomplished using scanning type sensors, which result in low hardware cost. Such hardware, which in most cases is the same as that used for attitude determination, eliminates the need for star maps or landmark recognition algorithms, thus minimizing the complexity of the onboard flight software.

Six orbit parameters are necessary to fully define a satellite's position and velocity. These parameters can be divided into two sets: the in-plane elements, which define the size and shape of the orbit and the satellite's position within the orbit, and those parameters which define the orientation of the orbit in inertial space. The in-plane set can be determined from Earth angular diameter measurements alone while the others require the sensing of two other celestial bodies in order to resolve all singularities. Thus, Earth, Moon and Sun sensing provide the necessary data for fully autonomous navigation.

Table 1. Satellite Autonomous Navigation History, from Chory (Ref. 1)

DATE (S)	AIR FORCE PROGRAM	MEASUREMENT TYPE (S)	MAJOR DEVELOPMENTS
1963-64	283	HORIZON SCANNING	NAVIGATION SYSTEM STRAPDOWN IMU TECHNOLOGY
1964	SSGS	HORIZON SCANNING; KNOWN/UNKNOWN LANDMARK TRACKING	VOLUMINOUS PERFORMANCE PREDICTIONS
1965	ULTRA	UNKNOWN LANDMARK TRACKING	ULTRA INSTRUMENT (PARTIAL COMPLETION)
1967-74	SPARS*	STRAPDOWN SLIT STAR SENSORS & STRAPDOWN GYROS	PROTOTYPE FOR DMSP
1970	STRETCH	HORIZON SCANNING	MORE PERFORMANCE PREDICTION
1970-73	ANT	KNOWN/UNKNOWN LANDMARK TRACKING INTERFEROMETER CONCEPTS	SYSTEM LEVEL REFINEMENTS; PARTIAL SENSOR DEVELOPMENT
1973-75	HANS	54 CONFIGURATION COMBINATIONS	PERFORMANCE PREDICTIONS; COMPARISON; SEXTANT, PASSIVE RANGING RECOMMENDATIONS
1976-79	HAARS*	STRAPDOWN MOSAIC (INCLUDING CCD) STAR SENSORS & STRAPDOWN GYROS	STRAPDOWN STAR SENSOR DESIGN SYSTEMS CONCEPT WITH 3 STAR SENSORS WITH AND WITHOUT STRAPDOWN GYROS
1977-81	ANARS	SEXTANT	FLIGHT TEST UNIT; ON-ORBIT PERFORMANCE
1979-85	MADAN	HAARS ATTITUDE SYSTEM, HORIZON SCANNING/OTHER NAVIGATION SENSORS	MADAN NAVIGATION SYSTEM DEVELOPMENT

*ATTITUDE REFERENCE SYSTEMS

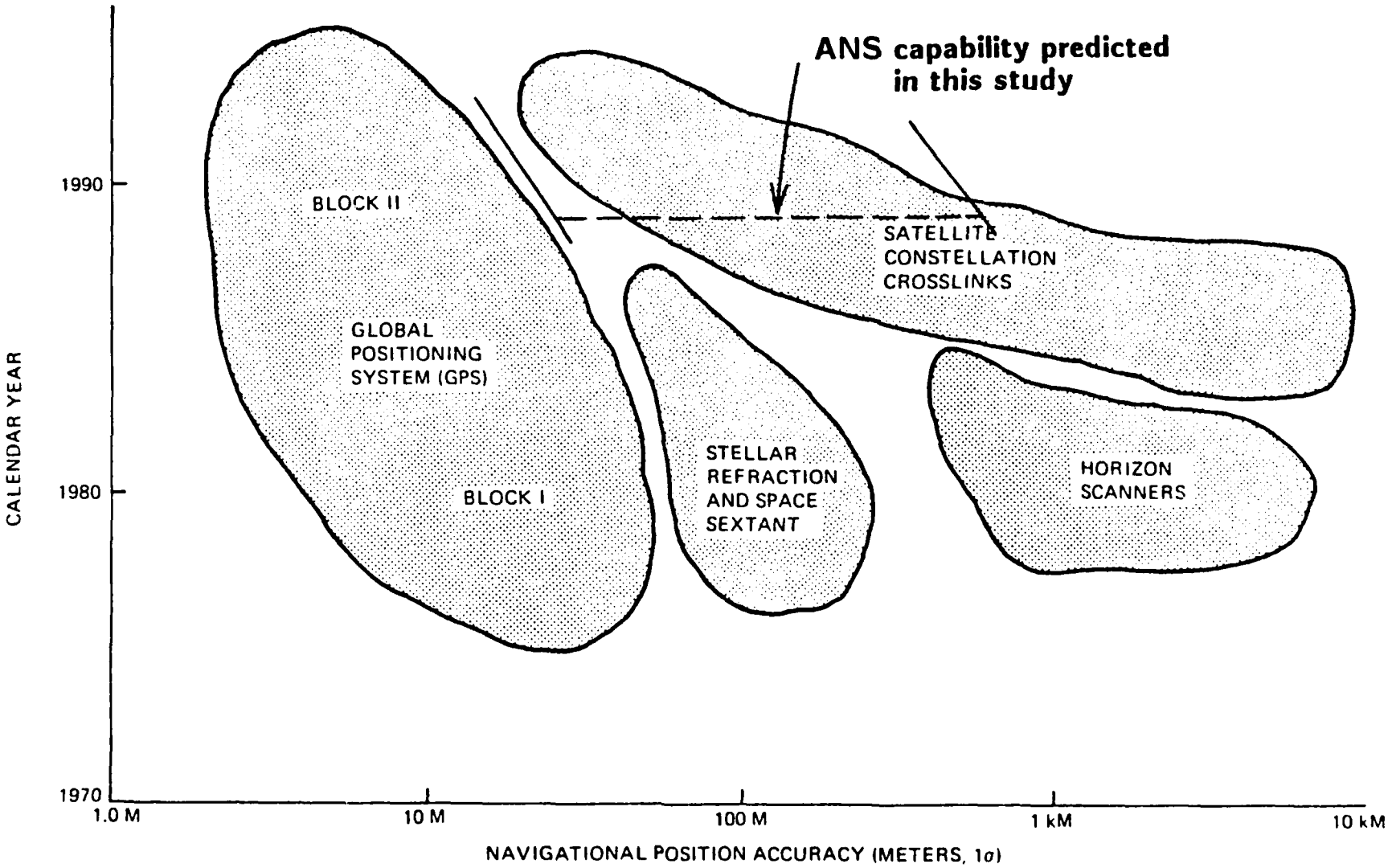

Figure 1. Overview of autonomous satellite navigation capabilities, from Chory (Ref. 1)

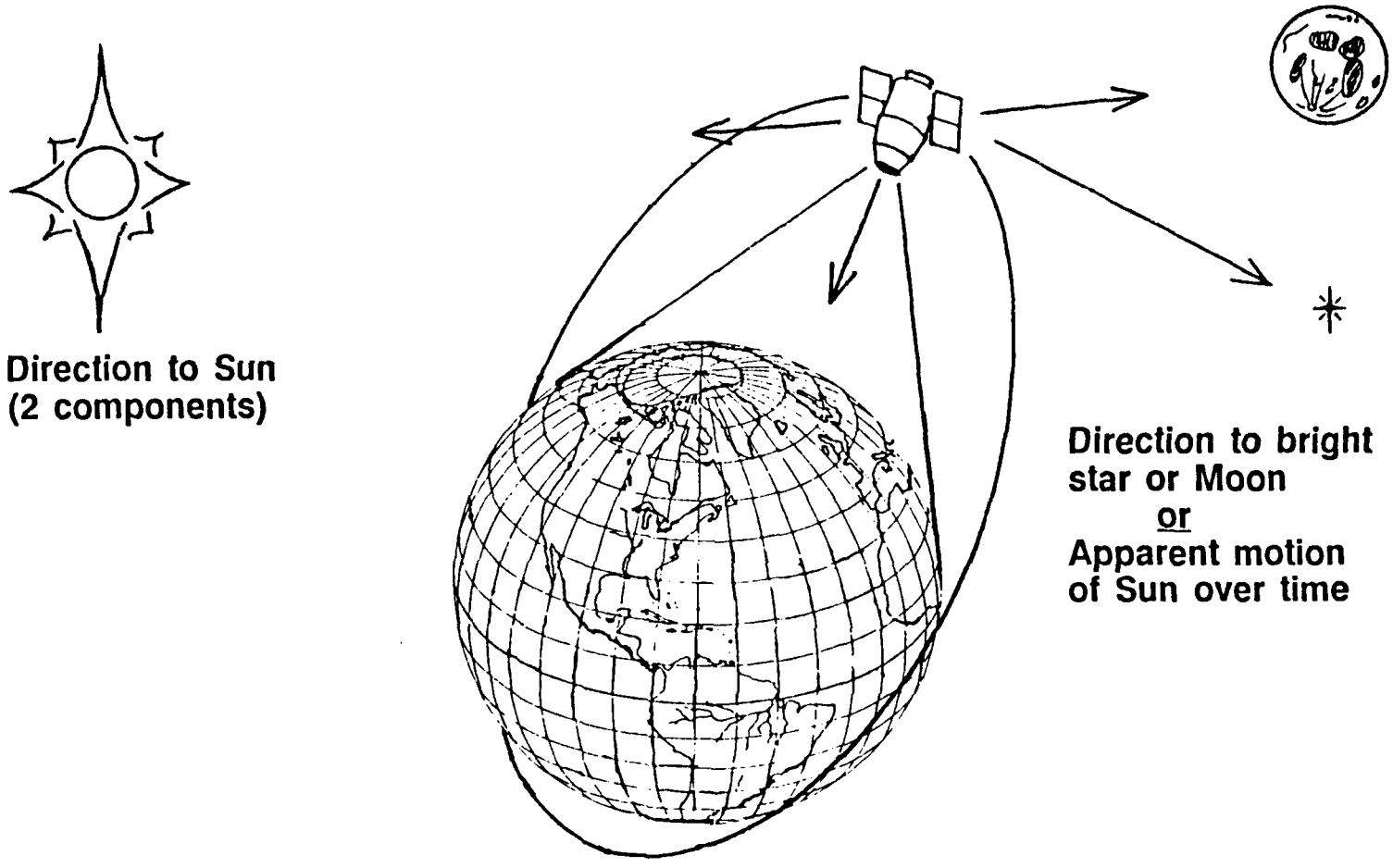

Figure 2. Independent measurements define orbit

Fig. 3 illustrates the traditional method of determining the in-plane parameters. Based on a minimum of three Earth angular radius measurements, estimates of the orbit radius, and the first and second derivatives of the orbit radius with respect to time are made. From these quantities, the semi-major axis (a), the eccentricity (e), and the mean anomaly (M) are computed. Additional measurements serve to refine the orbit.

Fig. 4 illustrates the traditional method of determining the plane of the orbit in inertial space. Using Earth, Sun and Moon observations, the satellite's position in inertial space can be determined. Using multiple observations, rates are defined. When combined with the in-plane information, the shape, size, and orientation of the orbit and the position of the satellite within the orbit are defined.

The Kalman filter (Section 5.1) provides an approach to implementing overall orbit determination. It calculates *corrections* to an extrapolated orbit as new data becomes available. Because it incorporates a continuum of measurements, the Kalman filter can in principle use data from a *moving* celestial body at two different *times* in place of *simultaneous* data from two different bodies. Thus, the Sun or Moon's apparent motion across the celestial sphere can be used to gradually resolve the ambiguity present in traditional two-body solutions.

Significant advantages are gained if navigation sensing is performed by a single sensor: the total number of sensors and therefore costs are reduced, the major source of systematic biases is eliminated thus improving overall accuracy, data interface requirements are minimized, and processing complexity is reduced. Existing conical Earth scanners can provide the accuracy necessary for determining the in-plane orbital elements. These sensors, which are typically flown on nadir pointing satellites like MSSP, would only require a small additional computational capability to produce the orbit data. The in-plane orbit elements and the orbit altitude are determined independently of the attitude of the system, using the methods covered above. (See Section 5.2.3) Figure 5 shows the altitude resolution as a function of the altitude for a typical conical scanner.

- Uses Earth angular radius information only
- Based on Taylor expansion near center observation
- Minimum of 3 observations necessary

Example: consider observations spaced at 10 minute intervals

- Uncertainty in radius observations is ±1 kilometer
- Only 3 observations were taken in this example

(Ordinarily many more data points would be available)

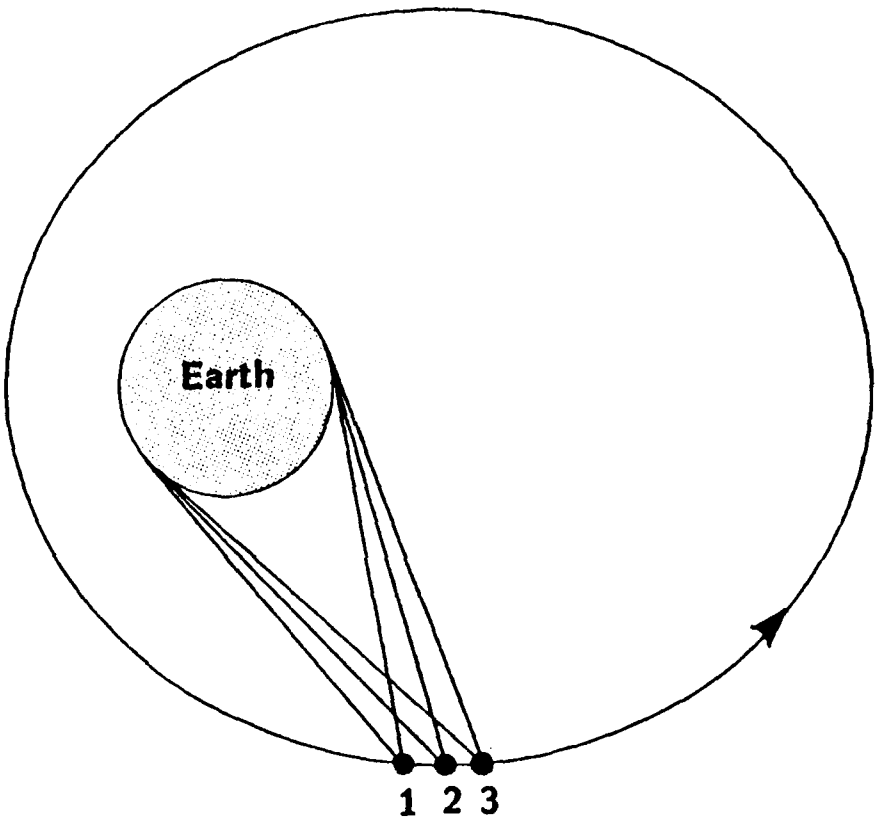

Element	Calculated	True
a	3.9827	4.0000
e	0.5008	0.5000
M	61.8075	61.3521

Figure 3. In-plane orbit determination

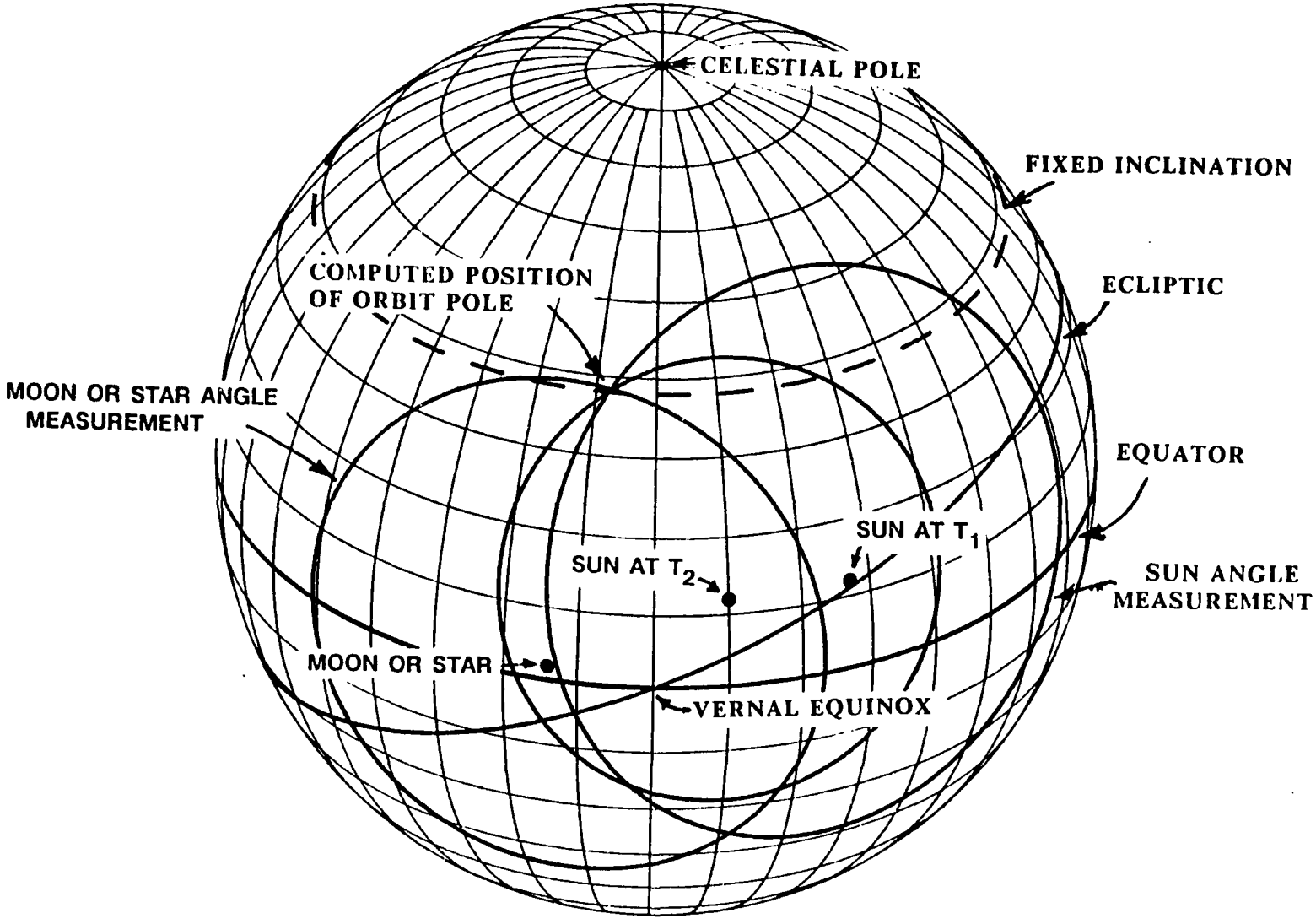

Figure 4. Sun and Moon measurements fix orbit orientation

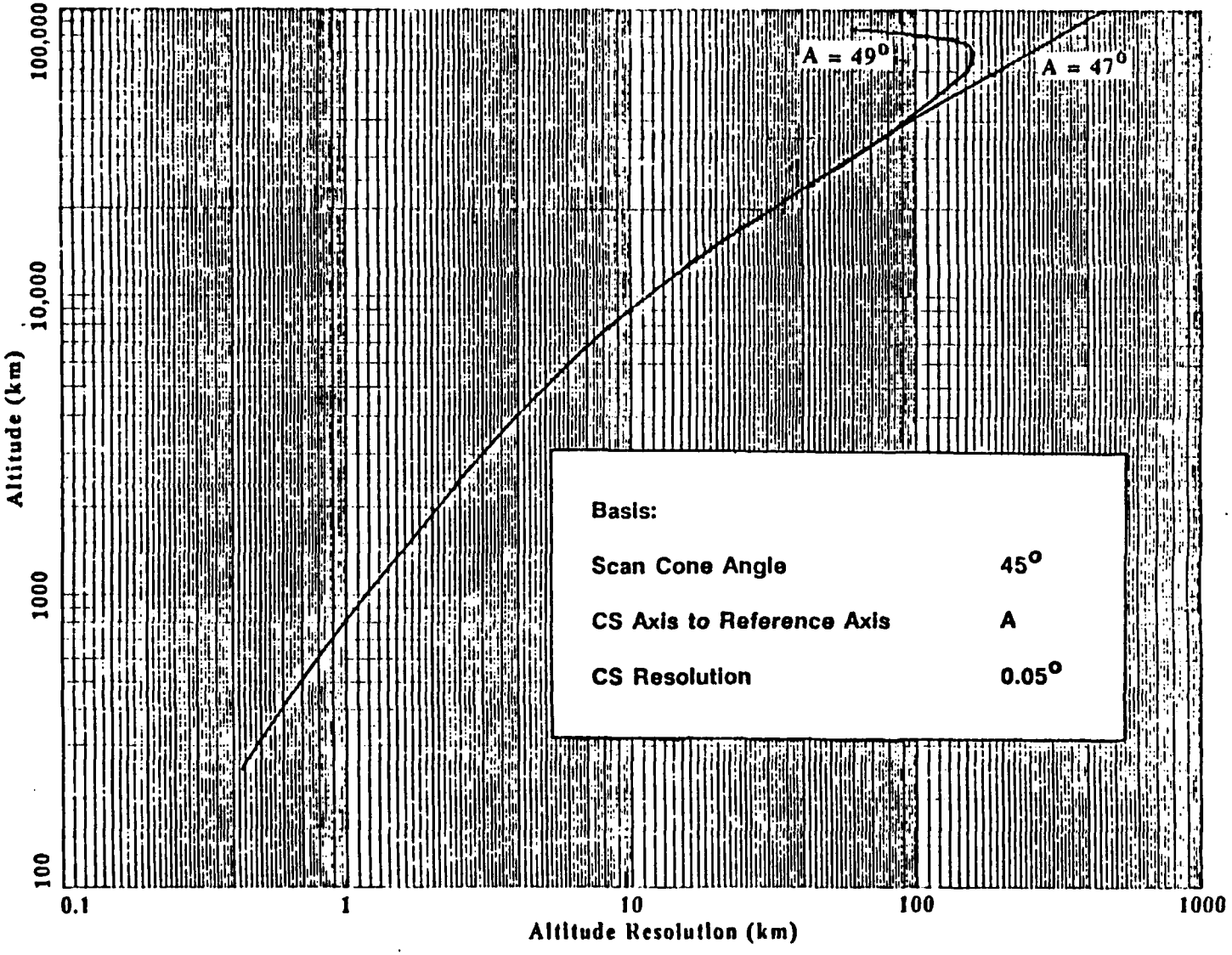

Figure 5. Conical scanner single scan altitude resolution

3. MSSP Mission Requirements

Concepts for the MSSP program have been studied by a number of contractors over the past five years. Several methods for controlling the satellites were investigated, including gravity gradient stabilization, implementing tuned masses, employing nutation dampers and adding momentum wheels. Table 2 gives the orbit and attitude ranges which resulted from these studies and were used in this study.

3.1. Satellite Orbit Requirements

For MSSP, a satellite constellation was established which would provide the necessary crosslinks and ground coverage. The number of satellites and their orbits, i.e., altitudes and inclinations, were key parameters. Table 2 gives the sets of orbit conditions recommended by the preliminary design study contractors. Although the selected altitudes remained relatively consistent, a wide range of orbit inclinations was selected to gain the necessary ground coverage. The Earth sensor can be adjusted to accomodate a wide range of altitudes with some trade-off between range and accuracy. Because of the narrow altitude range for MSSP, a sensor could be selected which would cover the entire range with no loss in sensing accuracy. Orbit inclination, however, affects the Sun/Moon-to-satellite angles, which, in turn, affect their attitude coverage and accuracy. These effects were studied parametrically and are discussed in Section 4.4.

3.2. Satellite Attitude Requirements

A number of control schemes were suggested by the contractors during the preliminary design phase. Table 2 summarizes their estimates of control capabilities. For the purposes of this study, the satellites were assumed to be nadir pointing, but unconstrained in yaw. Since the attitude and the orbit determination operations are independent, attitude control accuracy only indirectly affects navigation accuracy by affecting the amounts of Sun and Moon coverage and required range of Earth coverage. These effects are discussed later in Section 4.4.

The requirements for attitude determination are not derived from those for navigation. Navigation errors are propagated from the errors in sensing the Earth size and the angles between the Earth and the Sun and/or Moon. Attitude determination errors come from errors in sensing the directions to the Earth, Sun, and Moon. Since the combinations of data used for attitude determination are different from those used for navigation, attitude requirements are separable from navigation requirements. This results in much simplified autonomous navigation processing.

Attitude determination requirements can be estimated from the attitude control requirements generated by the preliminary phase A contractors. Table 2 gives the attitude control range of 2 to 20 degrees for MSS. Making allowances for control duty cycling and sensor misalignment, determination to within ± 0.5 degrees (3 sigma) will be sufficient to meet the minimum control requirement of 2 degrees.

TABLE 2: MSSP ATTITUDE CONTROL AND ORBIT SPECIFICATIONS

STUDY CONTRACTOR	ALTITUDE (nmi)	INCLINATION (deg)	NADIR CNTRL (±deg-3Σ)	YAW CNTRL (±deg-3Σ)	POS DETERM (km)
DARPA/RADC	400		10		autonomous, GPS, or ground track
LINKABIT	300-400	27.5,57.5,90		≤1 RPM	
CONTEL (grav grad)			10	none	
CONTEL (with M-wheel)	365	27.5,57,80	2	1	
RCA Astro (grav grad)	365-450	57-80	10	none	proportional to (time interval)^2
RCA Astro (tune masses)	365-450	57-80	6	20	
RCA Astro (damper)	365-450	57-80	3	20	
RCA Astro (M-wheel)	365-450	57-80	3	5	
RCA Astro (?)	365-450	57-80	6	7	
M/A-COM					10-20
BASD (grav grad)	338-365	57-80	10	1-2 RPM	
BASD (add M-wheel)	338-365	57-80	10	10	
BASD (+ M-bias, damp)	335-356		2	0.5-5.0	
TOTAL RANGES	335-450	27.5-90	2-10	.5-none	10-?

4. Sensor Hardware Configuration

4.1. The Autonomous Navigation Sensor (ANS)

The Autonomous Navigation Sensor (ANS) proposed for MSSP is a derivative of the Pan Axial Conical Scanner (PACS) manufactured by Barnes Engineering, Shelton, Connecticut. The PACS, which provides 3-axis attitude determination for three-axis stabilized spacecraft, is a conventional conical scanner which has been modified by adding a second Earth cone and a pair of fan sensors. The result is a sensor which is capable of detecting the Earth, Sun and Moon, and consequently provides all the information necessary to determine attitude and position.

The sensor employs a single, motor-driven optical scanning head with multiple fields of view sensitive to both the Earth's thermal radiance and the Sun's and Moon's visible light. The Earth and Sun fields of view are focused on and are therefore co-aligned within the single optical head. The sensor incorporates microprocessor-based electronic signal processing.

The ANS will have the same power and weight requirements as the units from which it is derived. This results in a total power estimate of 11 watts and weight estimates of 2.8 pounds for the sensor head and 5.5 pounds for the electronics. Fig. 6 shows the mechanical and optical configuration of the ANS.

4.2. Sensor Heritage

The ANS is based on flight proven components from previously flown sensors. It utilizes scan motors, bearings and lubrication systems from USAF/Lockheed Agena (and related) programs. It also employs pyroelectric infrared detectors from the Combined Earth Sensor for the USAF/Rockwell GPS/NAVSTAR program.

The Cosmic Background Explorer (COBE) mission uses a Planar Scan Horizon Sensor (90-degree half cone angle) which represents the starting point for the design of the ANS. Three straightforward modifications are made to the basic optical/mechanical design to achieve the enhancements in features and performance described herein. In addition, there are changes in the processing electronics and in the algorithms implemented in the associated microprocessor.

The single, rotating mirror used in the COBE sensor is split into two facets to create two separate Earth fields of view. The two halves are arranged to share the sensor aperture equally. The result is that the single infrared detector simultaneously scans two independent fields of view as shown in Fig. 7. The two FOV's are 180 deg out of phase and are at two independently chosen elevation angles, 60 and 80 deg.

To prevent sunlight from contaminating the Earth data, a silicon photodiode detector and germanium beam splitter are installed in the convergent optical beam just ahead

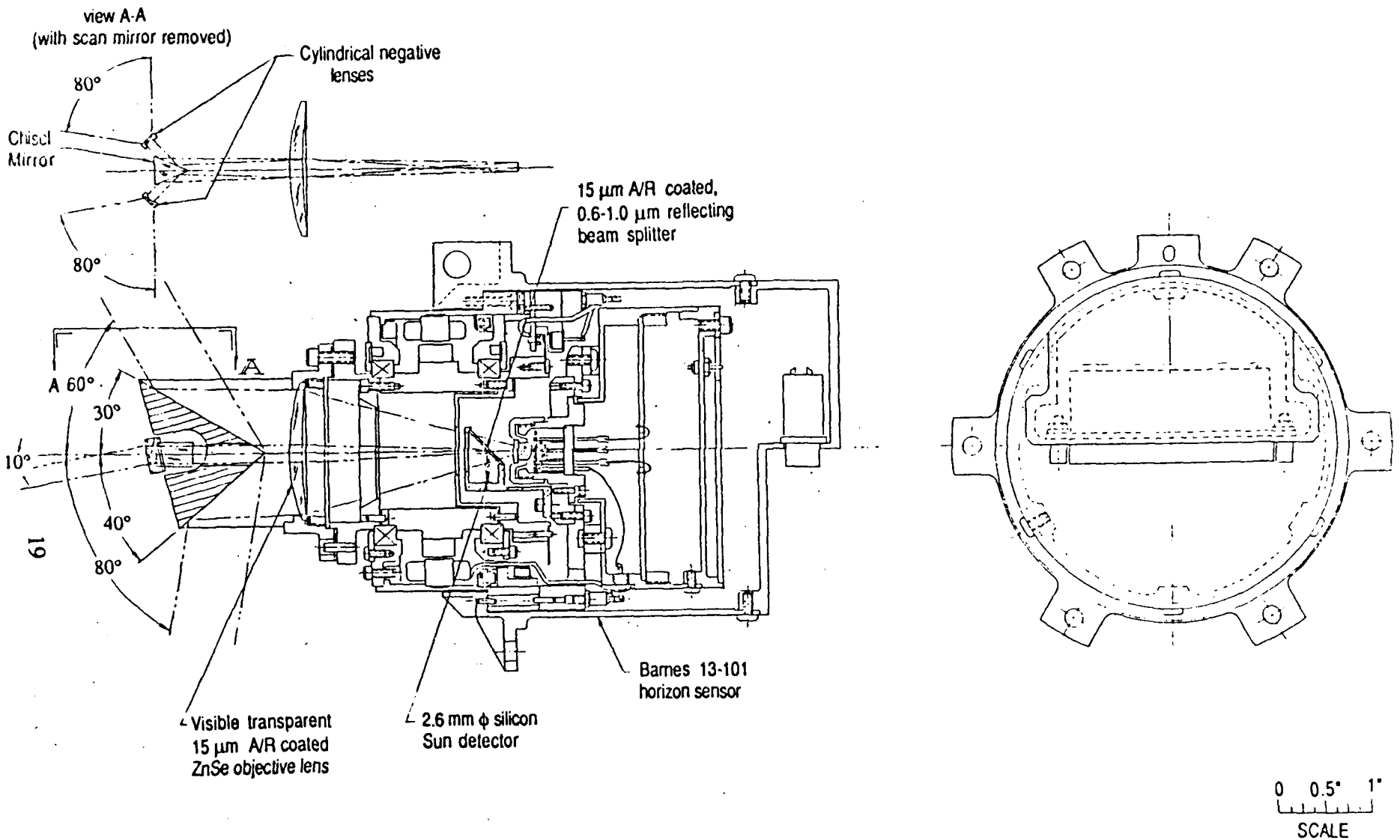

Figure 6. ANS mechanical/optical configuration (used with specific permission of Barnes Engineering, Division of EDO Corp., 25 July 1988)

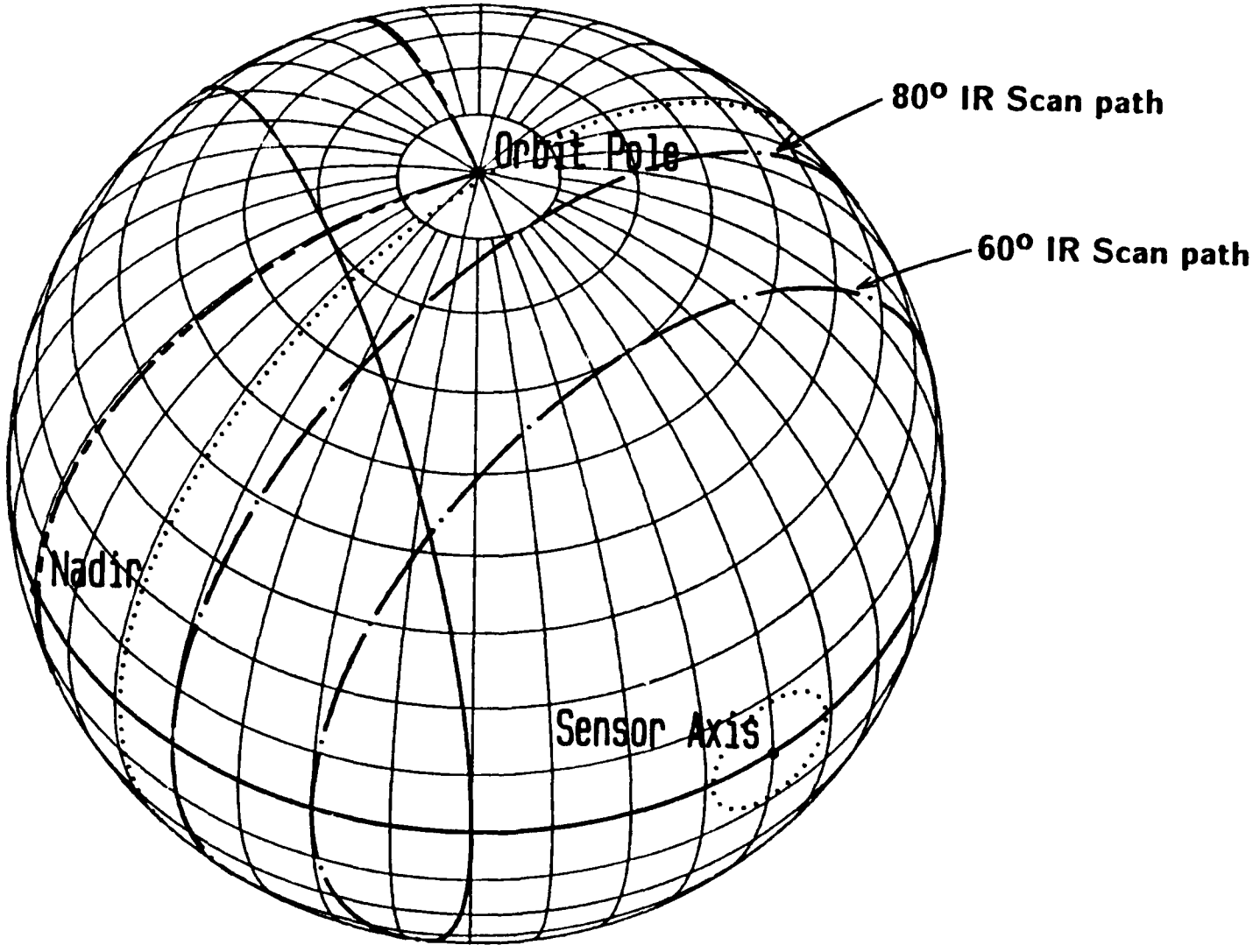

Figure 7. Single ANS IR fields of view

of the existing pyroelectric infrared detector/field lens assembly. The silicon detector subtends a circular "visible light" field of view slightly larger than the 2.5 degree pyroelectric detector's infrared field of view. Thus, it provides a guard band around the infrared field of view which determines the presence of the Sun when it is in or near the infrared field of view. Due to the intensity of the Sun's signal, the silicon detector can detect the Sun even when it is just rising or setting on the Earth's horizon.

The single field of view of a standard scanning Earth sensor will, from time to time, sweep across the Sun. While such sensors can discriminate between Earth and Sun crossings, substantial errors will occur when the Sun appears within a few degrees of the Earth's horizon. The ANS overcomes this problem by using the auxiliary visible light detector to sense when the Sun is near enough to one of the Earth crossings to cause interference. The uncontaminated crossings are selected to provide Earth data without any error due to the Sun's signal, even when the Sun appears at the horizon. When this occurs, the three of the four Earth crossings will be accepted as valid, and since three points define the circle they subtend, the altitude and attitude are still uniquely defined.

The same silicon detector described above is used to determine the attitude of the Sun or Moon. Provisions are made to give the visible light silicon detector a clear field of view through the scanning mirror and a direct view of the Sun or Moon at positions in the scan plane 90 degrees away from the nominal Earth crossings. As shown previously in Fig. 6, the silicon detector sees a small, 90 degree chisel-edged reflective mirror which splits this central 5mm field of view into two halves and directs them in opposite directions 90 degrees ahead of and 90 degrees behind the zero degree point in the scan plane. Each half is then expanded with a negative lens into a 90 degree wide fan-shaped field of view. The centerline of the chisel-edged mirror is set to tilt the fan-shaped fields 80 degrees with respect to the scan plane. When it rotates, it sweeps out an entire hemisphere minus a 10 degree cone about the spin axis. The sensor detects the presence of the Sun or Moon in the field of view and computes its two-axis attitude based on the timing of this data. The detector has multiple light intensity thresholds to distinguish between the Sun and Moon and for discrimination of the Earth. See Fig. 8 illustrating the sweeping fan sensor fields of view.

4.3. Sensor Scan Rate

The ANS employs the COBE microprocessor, which has the capability of processing two Earth horizon crossings every 0.25 seconds. Since the PACS employs two Earth cones, it detects four Earth crossings and twice the time will be required for processing. The same microprocessor is used for processing Earth and Sun/Moon data. The processor will be shared by detecting and processing Earth and Sun/Moon data on alternate sensor rotations. Based on the 0.50 second Earth data processing time given above, the sensor will rotate twice per second and Earth and Sun/Moon updates will each be provided once per second.

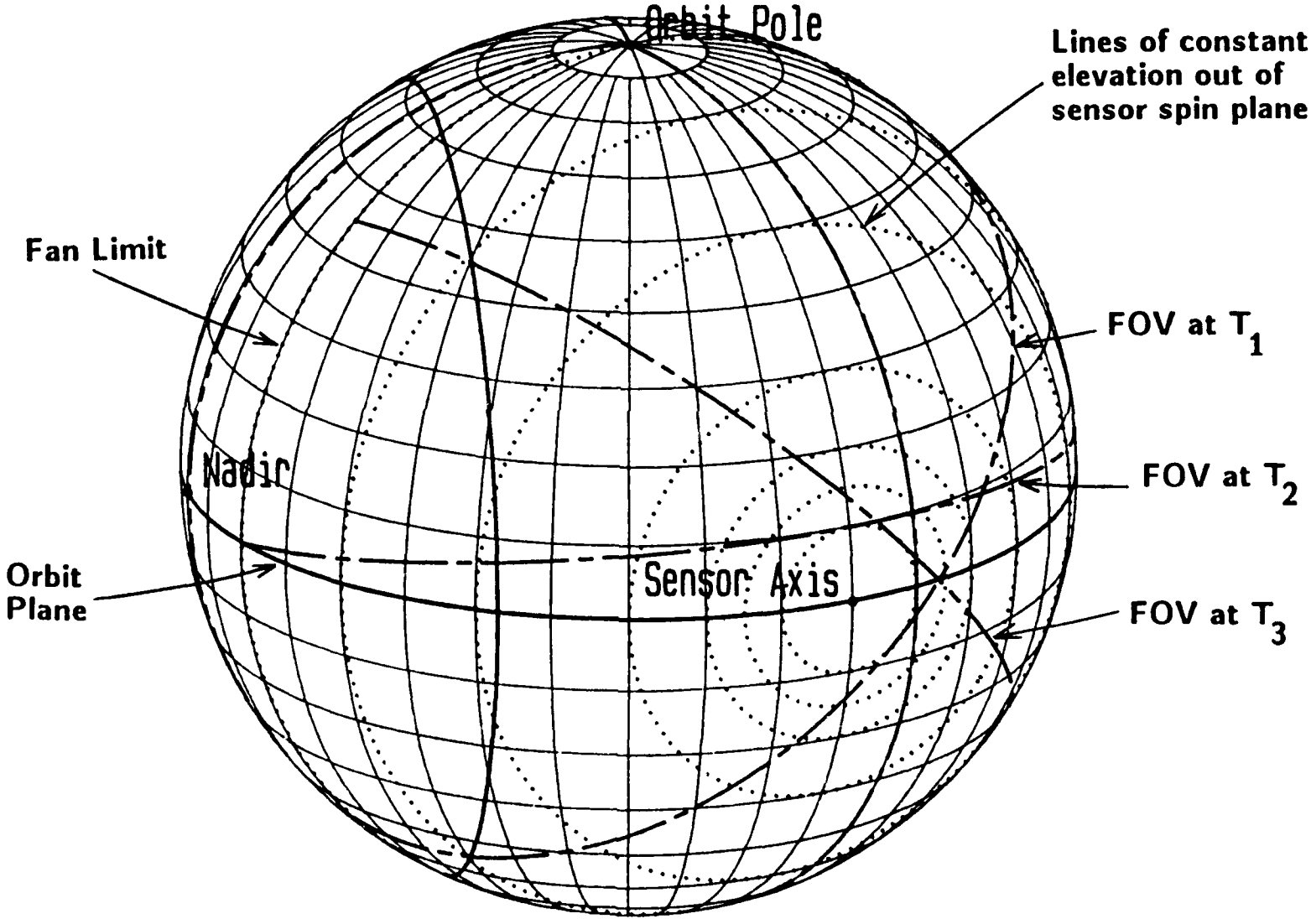

Figure 8. Sun/Moon fan fields of view

4.4. Sensor Mounting and Fields-of-View

Two sensing configurations have been evaluated for MSSP: a single ANS providing moderate performance at lowest cost, and a dual ANS configuration providing enhanced performance at moderate cost.

Mounting of the sensor(s) on the MSSP satellite was optimized to achieve maximum viewing of the Sun, Moon and Earth. Fig. 9 shows the mounting orientation for the dual ANS approach. For both sensors the rotation axis is 110° above nadir and in the orbit plane. The single ANS configuration will utilize one of the two sensors in the dual sensor layout. The infrared horizon sensing cone angles were selected to provide good Earth altitude and attitude sensitivity with wide ranges about the nominal 400 NMi altitude and nadir pointing attitude. The Sun fan limit and orientation were selected to provide the widest coverage of the Sun and Moon while considering Earth and satellite blockage.

Fig. 10 shows the path of the conical scans on the Earth for the nadir pointing MSS. Good Earth attitude and altitude data are collected for attitudes as high as 15 degrees in pitch and 90 degrees in roll. For MSS, which is nadir pointed to within 10 degrees, we therefore get continuous Earth radius and attitude data.

Fig. 8 showed the edge of the Sun/Moon fan as projected on the Earth and the celestial sphere for the nadir pointing MSS. Sun and Moon coverage can be expressed as a function of their elevation out of the orbit plane. Fig. 11 gives the percentage of total Sun or Moon coverage as a function of this elevation considering the MSS mounting angles, fan limits, altitude and Earth and satellite blockage. This coverage, one of the principal factors affecting overall navigation performance, was included in the analyses and simulations covered in this report.

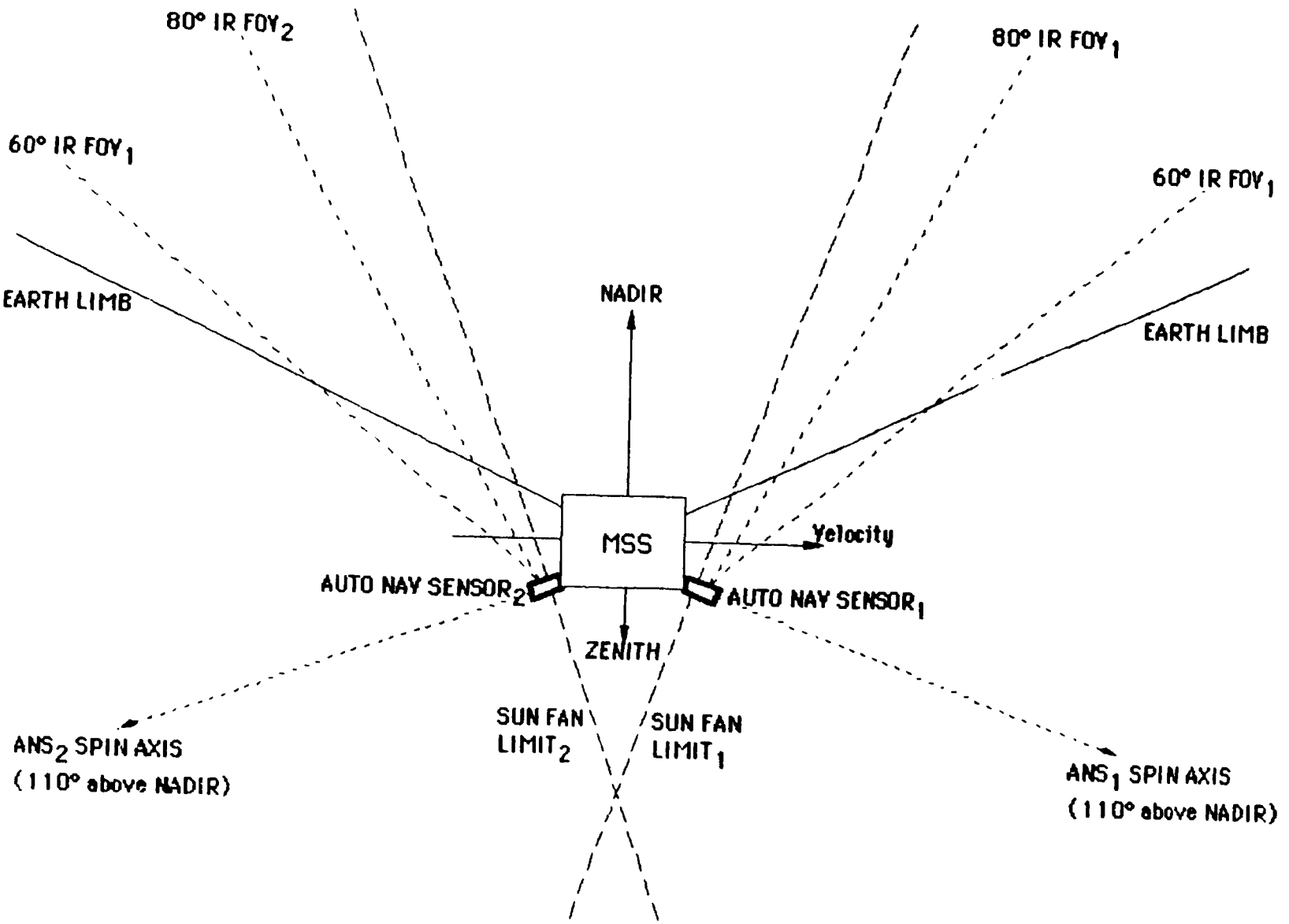

Figure 9. Sensor mounting on MSS

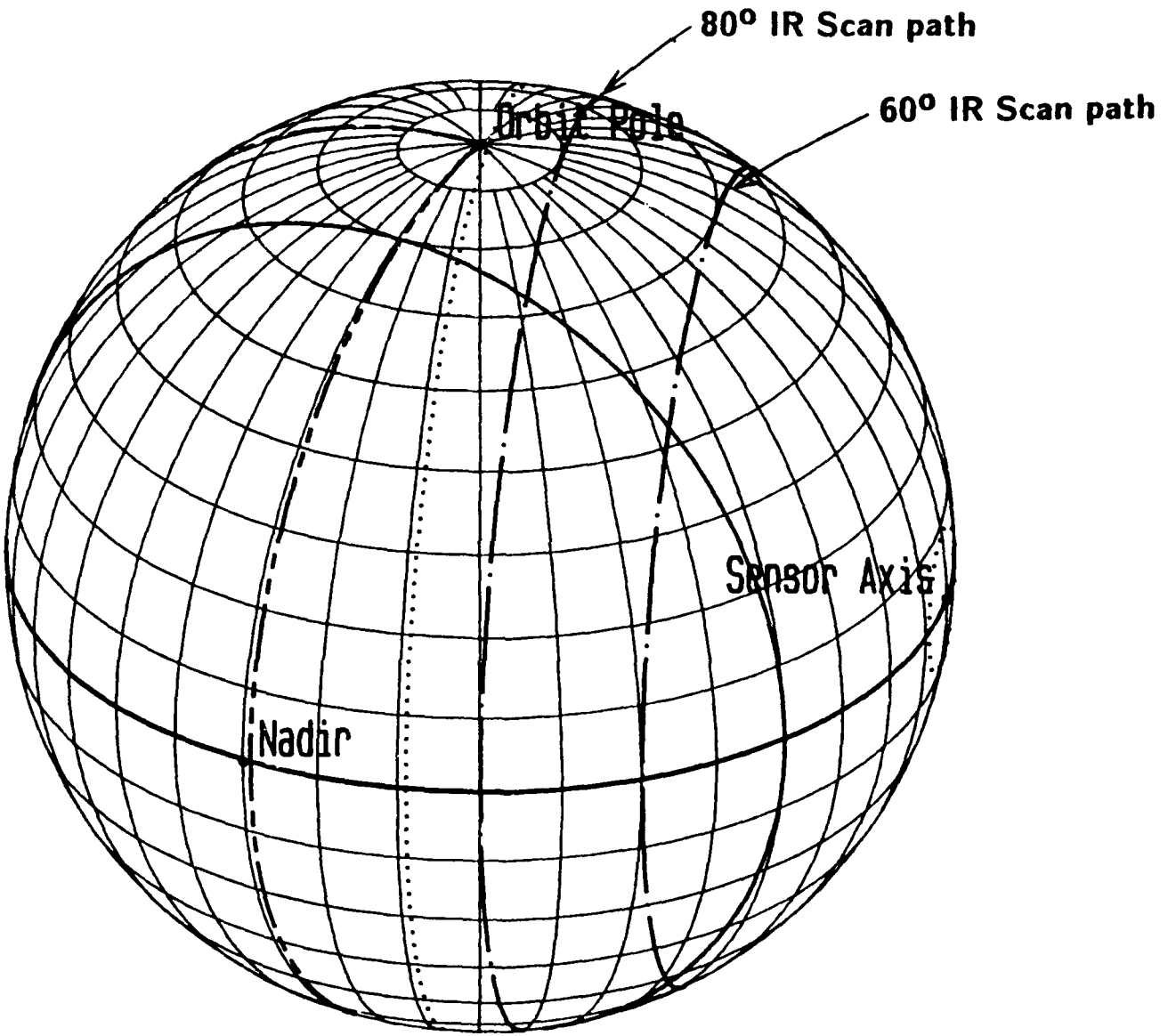

Figure 10. Single ANS Earth sensing

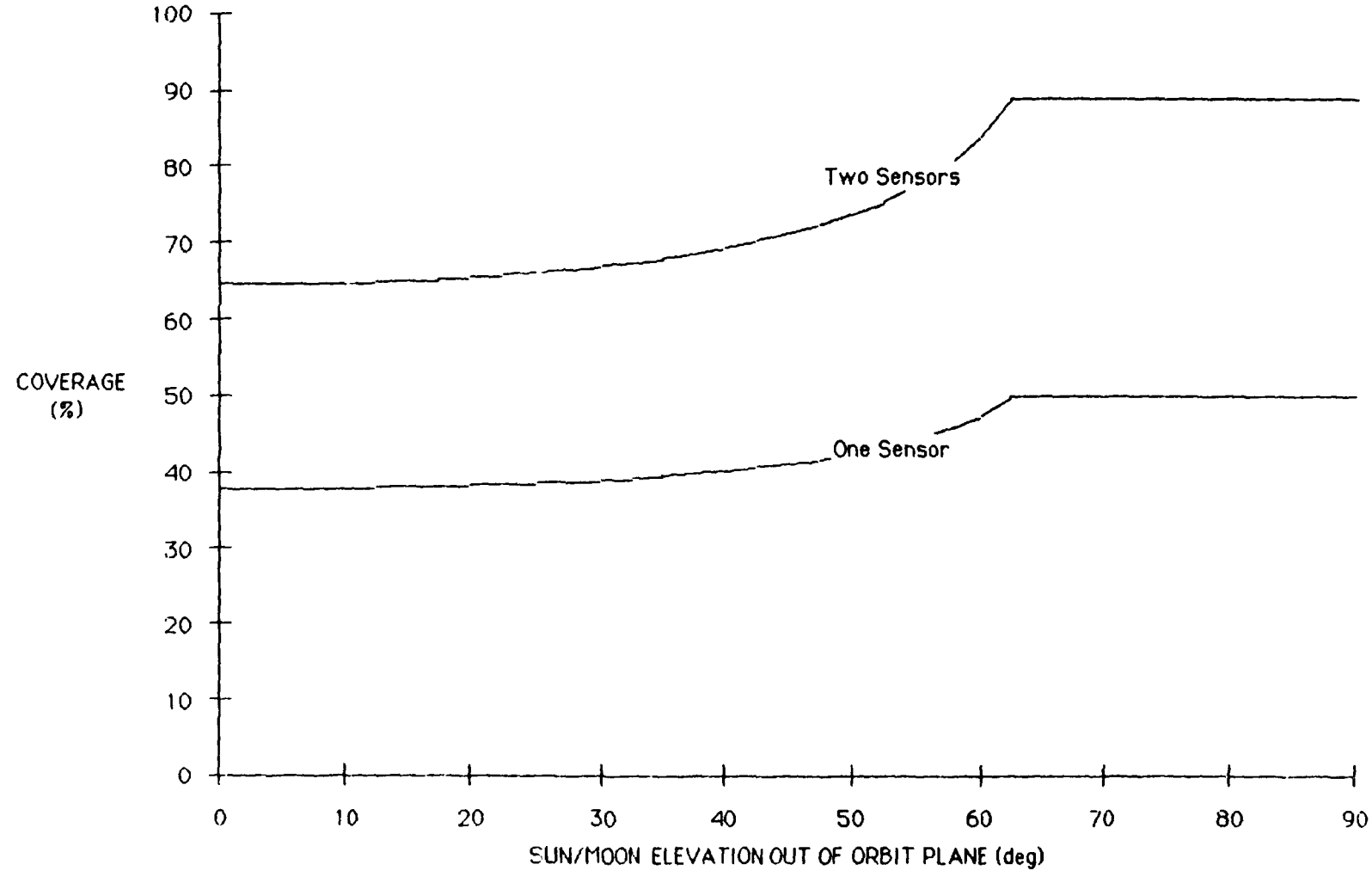

Figure 11. Sun/Moon coverage

5. Sensor Performance

5.1. Earth Sensing

The Earth data will contain systematic and random errors. Systematic errors cannot be reduced by averaging many observations but can be reduced by calibration. The random errors decrease like 1/sqrt(N) where N is the number of measurement points in a data set used as input to autonomous navigation filter (typically about 25). The principal error sources are described below.

5.1.1 Random Errors

The Earth pulse phase determines the azimuth of the horizon, i.e., the rotation angle of the sensor about its boresight. The phase error is 0.06 deg (3 sigma).

The Earth pulse width is the rotation angle between the horizon in-crossing and out-crossing. It determines the elevation of the sensor boresight. The times of the two crossings is differenced to determine the pulse width. The error in pulse width is 0.08 deg (3 sigma), including the RSS'ing of the two edges.

The azimuth error for the dual scan cone is directly proportional that of the pulse phase. The errors for Earth radius (implicitly--for altitude) and for elevation are obtained by dividing the errors in pulse width by the theoretical dual scanner gains. These are obtained as follows: Equation (11-39) of Wertz (Ref. 4) relates the Earth radius *rho*, the elevation *eta*, the cone angle *gamma*, and a single scan Earth width (arc along the scan cone) *omega* by:

$$\cos(rho) = \cos(gamma_i) * \cos(eta) + \sin(gamma_i) * \sin(eta) * \cos(omega_i/2) \quad (1)$$

If we apply this twice for i = 1, 2 and define

$$u_i = \mathrm{sqrt}\{\cos^2(gamma_i) + [\sin(gamma_i) * \cos(omega_i/2)]^2\}, \quad (2a)$$

and

$$x_i = \sin(gamma_i) * \cos(omega_i/2)/u_i, \quad (2b)$$

we can solve for the pitch as

$$\tan(eta) = \{\cos(gamma_2) - \cos(gamma_1)\}/\,\mathrm{den}\,, \quad (3)$$

where

$$den = \sin(gamma_1) * \cos(omega_1/2) - \sin(gamma_2) * \cos(omega_2/2) \quad (4)$$

and for the Earth radius from

$$\cos(rho) = |\sin(x_1 - x_2)| * u_1 * u_2/den2\,, \quad (5)$$

where

$$den2 = \mathrm{sqrt}[u_1 * u_1 + u_2 * u_2 + 2 * u_1 * u_2 * \cos(x_1 - x_2)] \quad (6)$$

The gains are obtained by differentiating these expressions. They are shown in Figs. 12 and 13 for 1 and 2 sensors, respectively.

Table 3 gives the dual scanner gains for our configuration. They are used to convert nominal measurement errors within a scan into accuracies in Earth centroid position. The dual ANS is treated as a single dual scan sensor with half cone angles of 60° and 160° representing one scan from each of the sensors. This is conservative and we could assume another factor 1.414 improvement from the additional two scans provided by the two sensors.

Table 3: Dual Scan Gains

	Elevation gain	Radius gain
Single ANS	0.70	1.10
Dual ANS	4.7	5.2

If we apply these gains to the stated accuracy of 0.06 deg in pulse phase and 0.08 deg in pulse width and allow for repeated measurement we can find the accuracies for centroid position and for Earth radius. Taking into account the averaging over 25 measurements for a typical navigation filter input, we get the accuracies shown in Table 4.

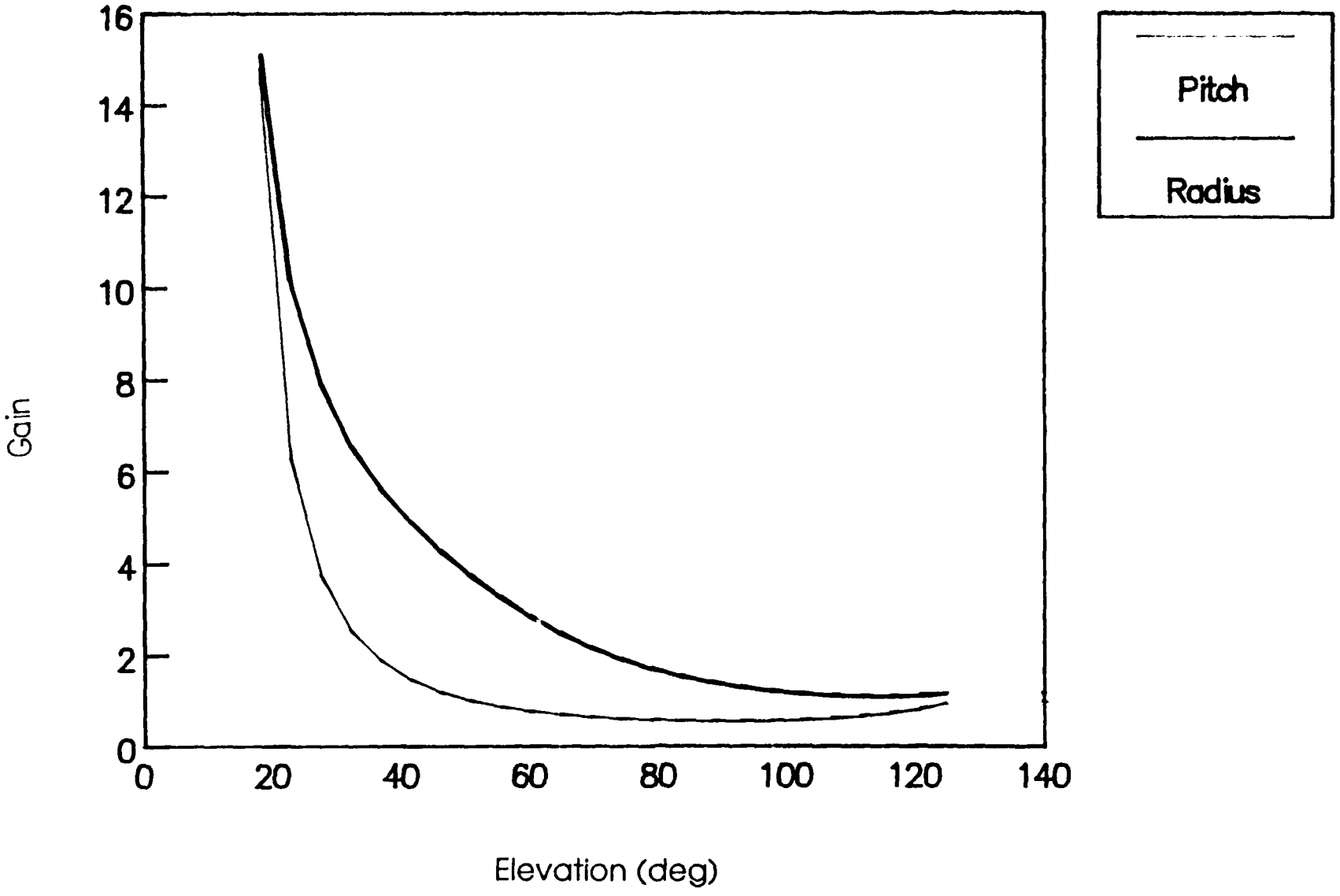

Figure 12. Dual Earth scanner gains for single ANS

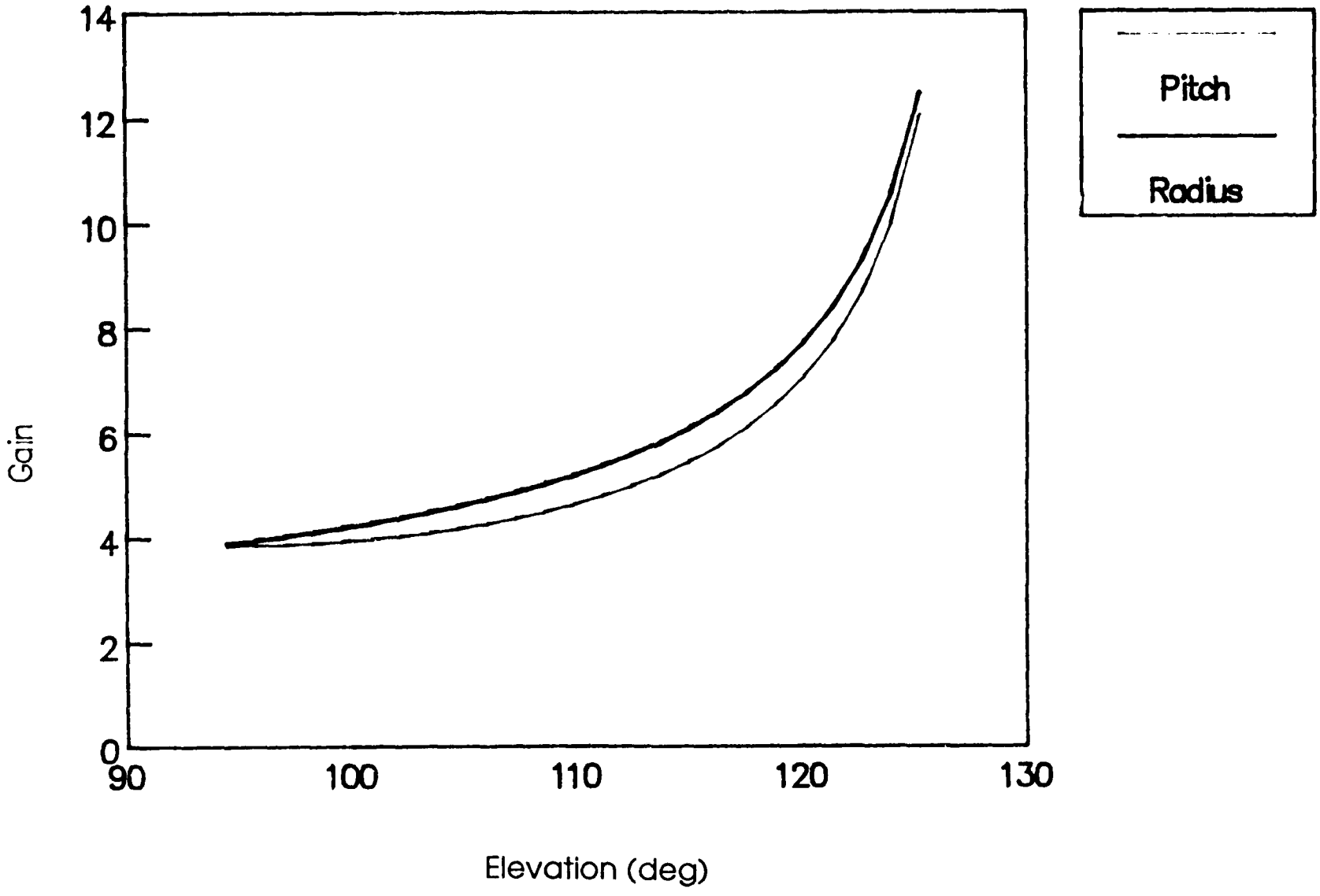

Figure 13. Dual Earth scanner gains for two ANS

Table 4. Earth Errors

	Centroid Elevation (deg 3 sigma)	Centroid Azimuth (deg 3 sigma)	Radius (deg 3 sigma)
Single ANS	0.026	0.011	0.017
Dual ANS	0.0038	0.0084	0.0033

5.1.2 Systematic Errors

A major advantage of the ANS is that Earth, Moon, and Sun measurements are all made with a single sensor. This serves to eliminate the inter-sensor mounting angle biases which are the major systematic error sources in multi-sensor autonomous navigation schemes. The principal sources of residual systematic errors in the autonomous navigation system are:

- Unmodeled forces in the orbit propagator
- Omitted terms in the on-board Sun and Moon ephemeris
- Internal residual mounting angle errors
- Unmodeled timing errors between observations
- Systematic bias on the Earth's angular radius due to triggering height uncertainty

We anticipate that the low cost, near-term autonomous navigation solutions will be dominated by the unmodeled forces on the orbit. During the current study, several cases were run with forces included in the data simulator which were not modeled in the Kalman filter, thus simulating the effect of unmodeled forces. The principal goal of these tests was to determine the stability and convergence characteristics of the Kalman filter. Results of these tests indicate that with an appropriate level of process noise, the Kalman filter is able to successfully track the orbit in spite of the presence of unmodeled forces. Thus, the preliminary conclusion is that the process is able to accommodate a reasonable level of systematic error. Further testing is desirable, but is beyond the scope of the current study.

In a fully implemented autonomous navigation system, the final position error will almost certainly be dominated by one or more of the systematic error sources. This is because the long term filtering process will drive the random component of the error below the level of the residual systematic

terms. All of the bias sources listed above are subject to being reduced by one of several processes:

- More detailed on-board model for orbit and ephemerides
- Improved sensor ground calibration
- On-orbit bias determination from the ground with bias parameters sent to on-board model
- Inclusion of additional terms in on-board filtering process

Thus it is possible to substantially reduce the systematic error terms, and, consequently, improve the accuracy of the final autonomous navigation solution. The level to which this is done will depend on the cost versus accuracy trade for the mission to which the system is ultimately applied.

5.2. Sun and Moon Sensing

The ANS outputs data on the timing of its intersections with the Sun or Moon. When the Sun or Moon is in the sensor spin plane, the two inter-sections per revolution will be equally spaced. Because of the tilt of the sensor fan, as the Sun's or Moon's elevation out of the sensor spin plane increases, the two intervals become increasingly unequal. At its limit (at a Sun or Moon sensor elevation of 80 degrees), the two intersections reduce to one. In Fig. 8, one sees this effect by observing the separation of the intersections of the fan with different elevation lines.

5.2.1. Sun/Moon Azimuth Determination

The azimuth of the Sun/Moon is the measurement of its angle about the rotation axis of the sensor. It is defined relative to a fiduciary mark on the sensor corresponding to a fiduciary timing signal, $T_{fiduciary}$. The azimuth angle of the Sun/Moon is computed as follows:

$$\text{Azimuth} = (0.5 * (T_{fan_1} + T_{fan_2}) - T_{fiduciary}) * 360^\circ/(\text{Spin Period})$$

5.2.2. Sun/Moon Elevation Determination

The elevation of the Sun/Moon is the angle of the line to the Sun/Moon with respect to the sensor spin plane. It is derived from the timing data by first determining the phase separation between the Sun/Moon as detected by the two fans. Figure 14 shows the celestial sphere centered on the sensor and the angle *alpha* which is half the difference between 180° and the phase difference between the detections. *Alpha* is computed as follows:

$$alpha = 0.5 * (180^\circ - (T_{fan_1} - T_{fan_2}) * 360^\circ / \text{Spin Period})$$

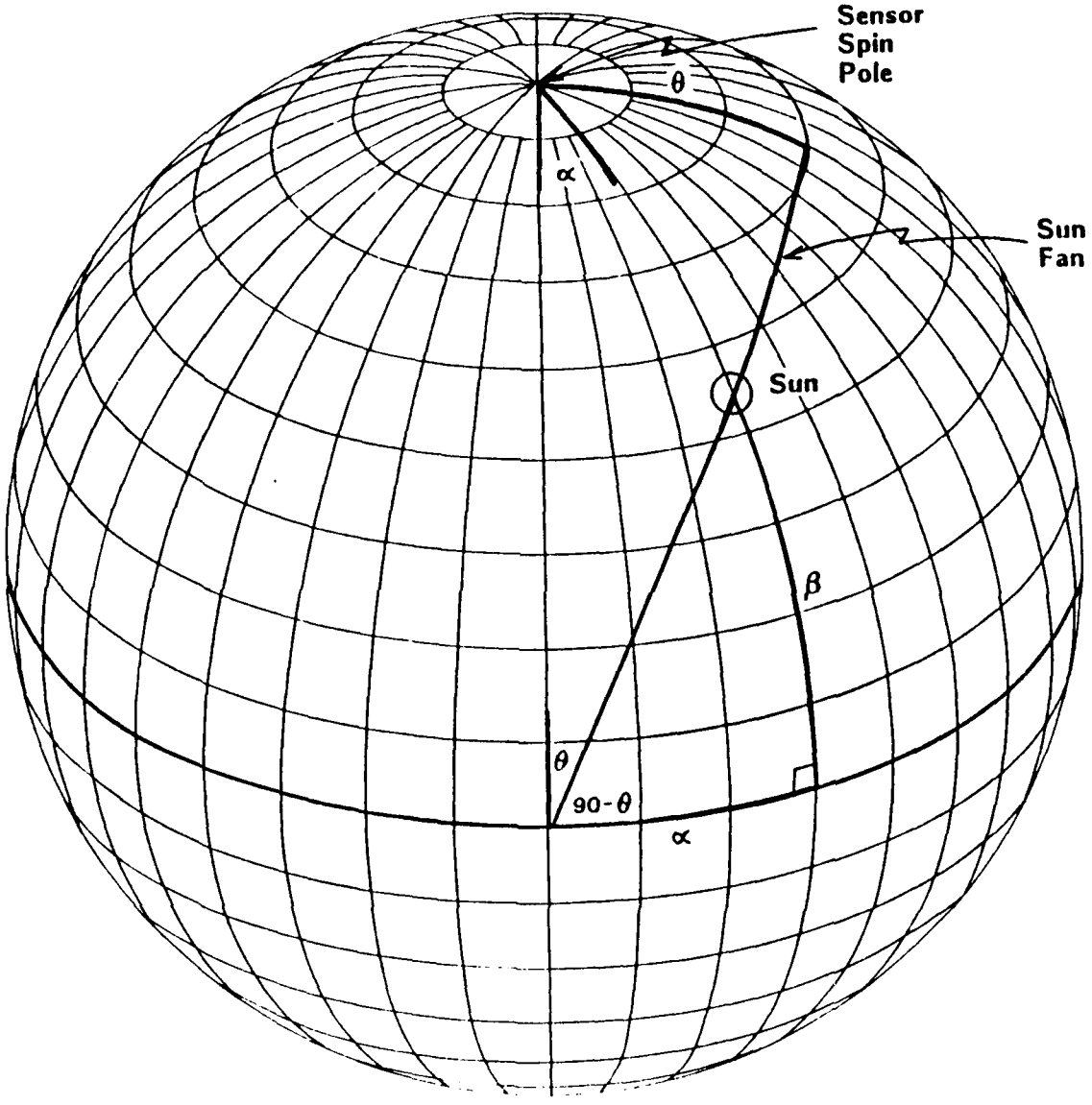

Figure 14. Fan sensor measures beta and alpha

Fig. 14 also shows the Sun or Moon, at elevation *beta*, as detected by the fan, tilted at angle *theta*. Using spherical geometry techniques, *beta* can be computed as a function of *alpha* and *theta* as follows:

beta = arctan (sin(*alpha*) / tan(*theta*))

Fig. 15 shows the relationship between *alpha* and *beta* for the 10° fan sensor tilted at theta = 10°.

5.2.3. Sun Azimuth Accuracy

Because of the extreme signal strength of the Sun, there is no change in sensor accuracy due to changes in the angle of attack between the Sun and the fan. The azimuth accuracy of the Sun for a single detection is .01° (3-sigma). The principal error sources in detecting the Sun are of the random or noise type and therefore this error is reduced when multiple measurements are made and then averaged. Since the navigation algorithm will be updated less often than once per second, the Sun attitude data will be averaged and their error will be reduced by the inverse square root of the number of measurements. Therefore:

Sun azimuth error = .0707° /sqrt (update interval)

5.2.4. Sun Elevation Accuracy

Because the Sun's elevation relative to the sensor spin plane (*beta*) is determined from the angle *alpha* and the geometrical relationship between *alpha* and *beta*, its accuracy, in turn, becomes a function of the accuracy of *alpha* and the *beta(alpha)* function. Taking the derivative of this function (given above in Section 5.2.2) with respect to variations in *alpha* results in the following:

$$d(beta)/d(alpha)=(\tan(theta) * \cos(alpha)) / (\tan^2(theta) * \sin^2(alpha))$$

Multiplying this by the .001° (3-sigma) error in *alpha* results in the Sun elevation accuracy plot shown in Fig. 16. Consistent with the reduction in azimuth accuracy due to averaging, elevation error also reduces by the inverse square-root of the number of measurements. Fig. 16 also shows the elevation-independent azimuth accuracy and the total Sun accuracy found by RSSing the two.

5.2.5. Moon Azimuth Error

Like the Sun, the major error contributors to the Moon sensing process are considered to be random or noise-type. Unlike the Sun, the angle of attack between the Moon and the fan has a significant effect on the Moon's

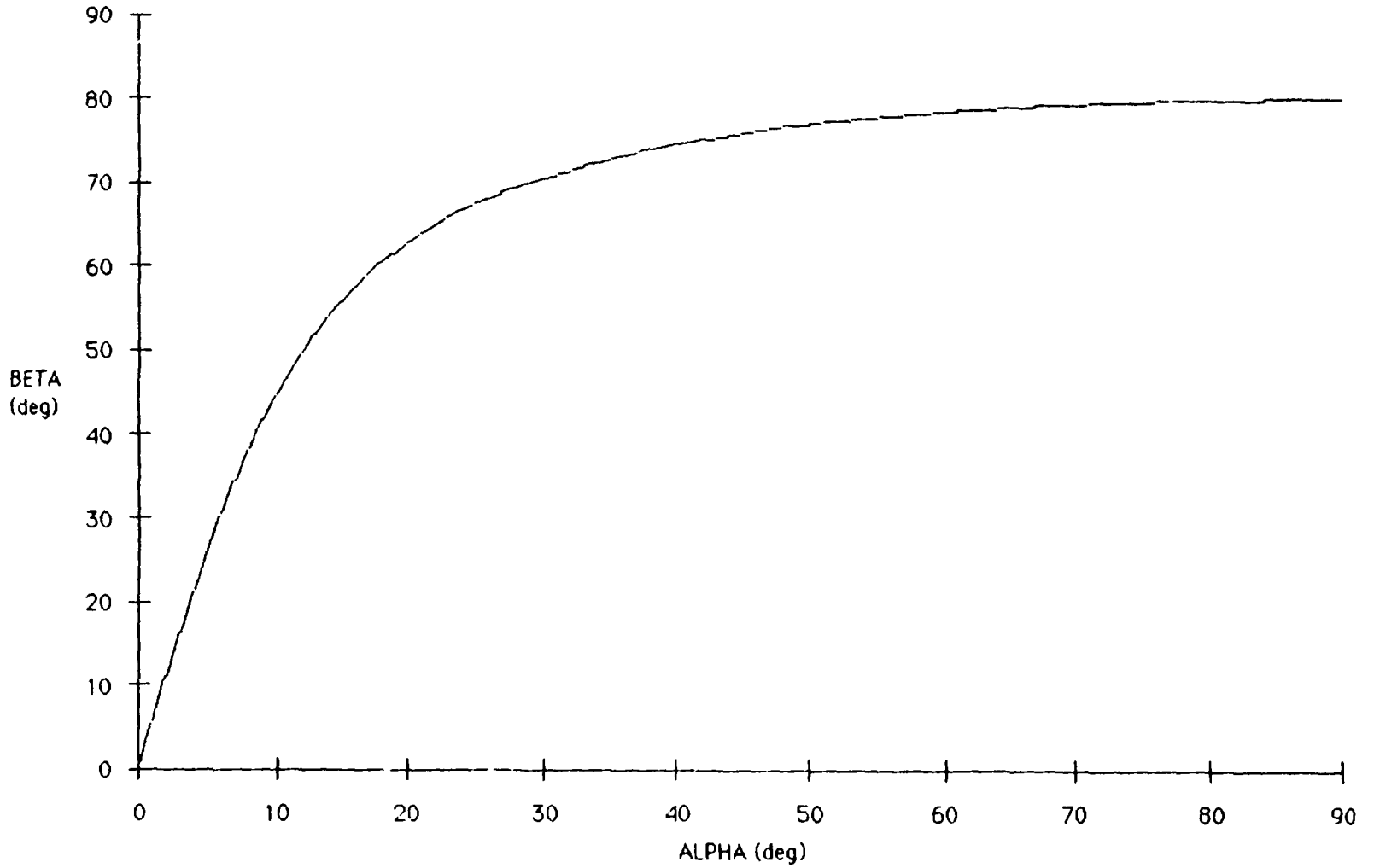

Figure 15. Beta/alpha relationship

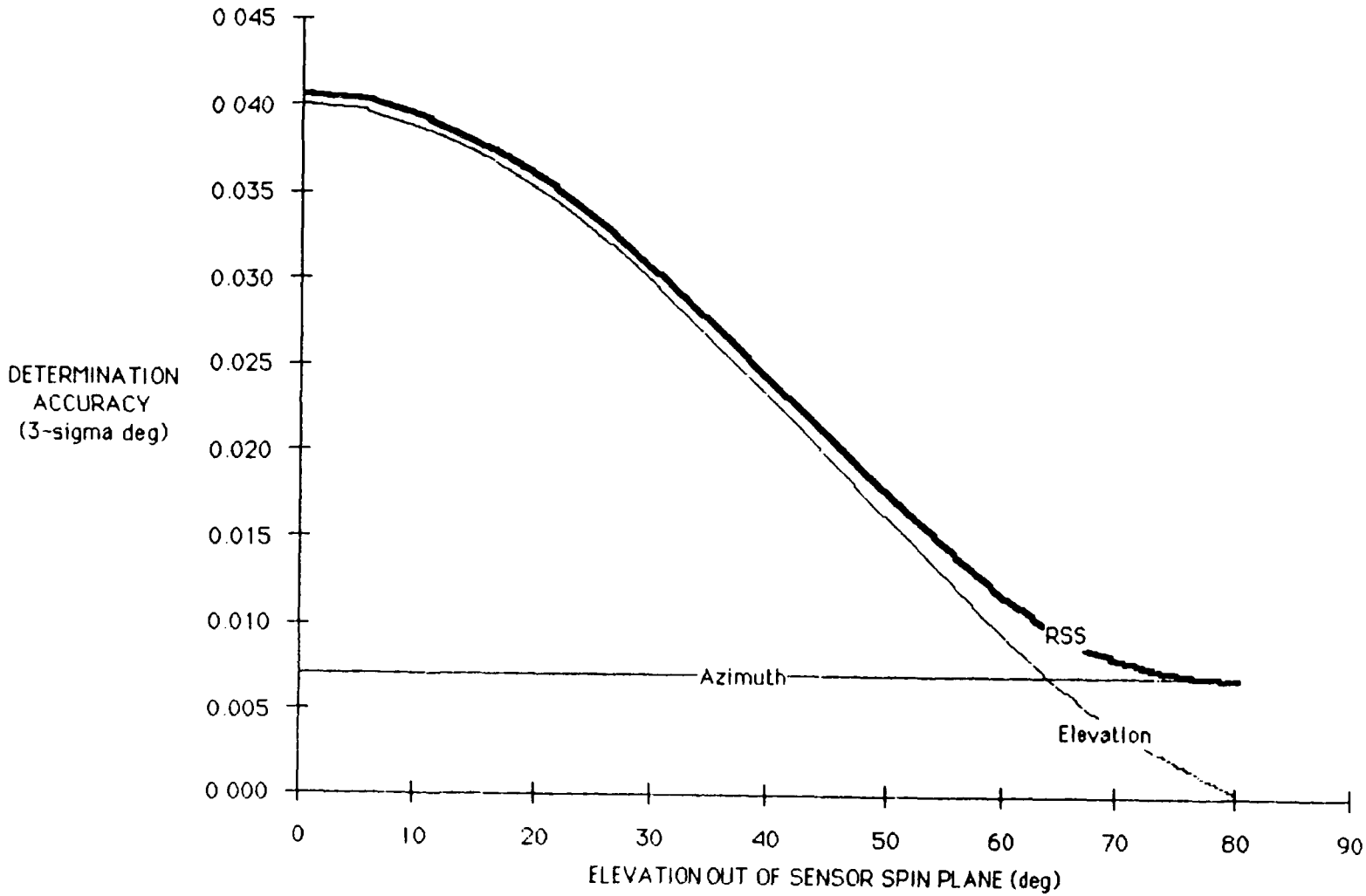

Figure 16. Sun attitude accuracy

accuracy because of its lower visible light intensity. This accuracy change is found to vary inversely with the cosine of the angle of attack. In Fig. 14, the angle of attack (AA) is the remaining angle in the spherical triangle. . From spherical geometry techniques, AA is found to be a function of *alpha* and the fan tilt (*theta*) as follows:

$$\cos(AA) = \cos(alpha) * \cos(theta)$$

Using the .05° (3-sigma) error per detection specified for the Moon and accounting for the improvement for averaging the two data points (for fan 1 and fan 2), the following azimuth error per sensor rotation, or per second, results:

$$\text{Moon azimuth error} = .05^\circ/(\text{sqrt}(2) * \cos(alpha) * \cos(theta)) = .0354^\circ/(\cos(alpha) * \cos(theta))$$

Fig. 17 shows the variation in Moon azimuth error with its elevation out of the sensor spin plane. As mentioned above, the principal error sources in detecting the Moon are of the random or noise type and therefore this error decreases by the inverse square-root of the number of measurements taken between updates.

5.2.6. Moon Elevation Accuracy

Because the Moon's elevation relative to the sensor spin plane (*beta*) is determined from its angle *alpha* and the geometrical relationship between *alpha* and *beta*, its accuracy becomes a function of the accuracy of *alpha* and the *beta(alpha)* function. Using the derivative of this function (given above in Section 5.2.2) and multiplying it by the *alpha* accuracy function derived in the previous section results in the following Moon elevation error:

$$\text{Moon elevation error} = .0354^\circ * \sin(theta)/(\cos^2(theta) * \tan^2(theta) * \sin^2(alpha))$$

Fig. 17 illustrates this error as a function of the Moon's elevation. Consistent with the reduction in azimuth error due to averaging, elevation error reduces by the inverse square-root of the number of measurements between updates. Fig. 17 also shows the RSS combination of the two.

5.3. Overall Interobject Accuracies

The results from the Earth, Sun, and Moon sensors are combined to get overall accuracies. As described in Sect. 4.3, the sensor will provide one set of data (Sun, Moon, and Earth positions, attitude, and Earth radius) per second. These observations will be averaged over an update interval, dt, before being fed to the Kalman filter. There are several reasons for this preprocessing. First, to run the

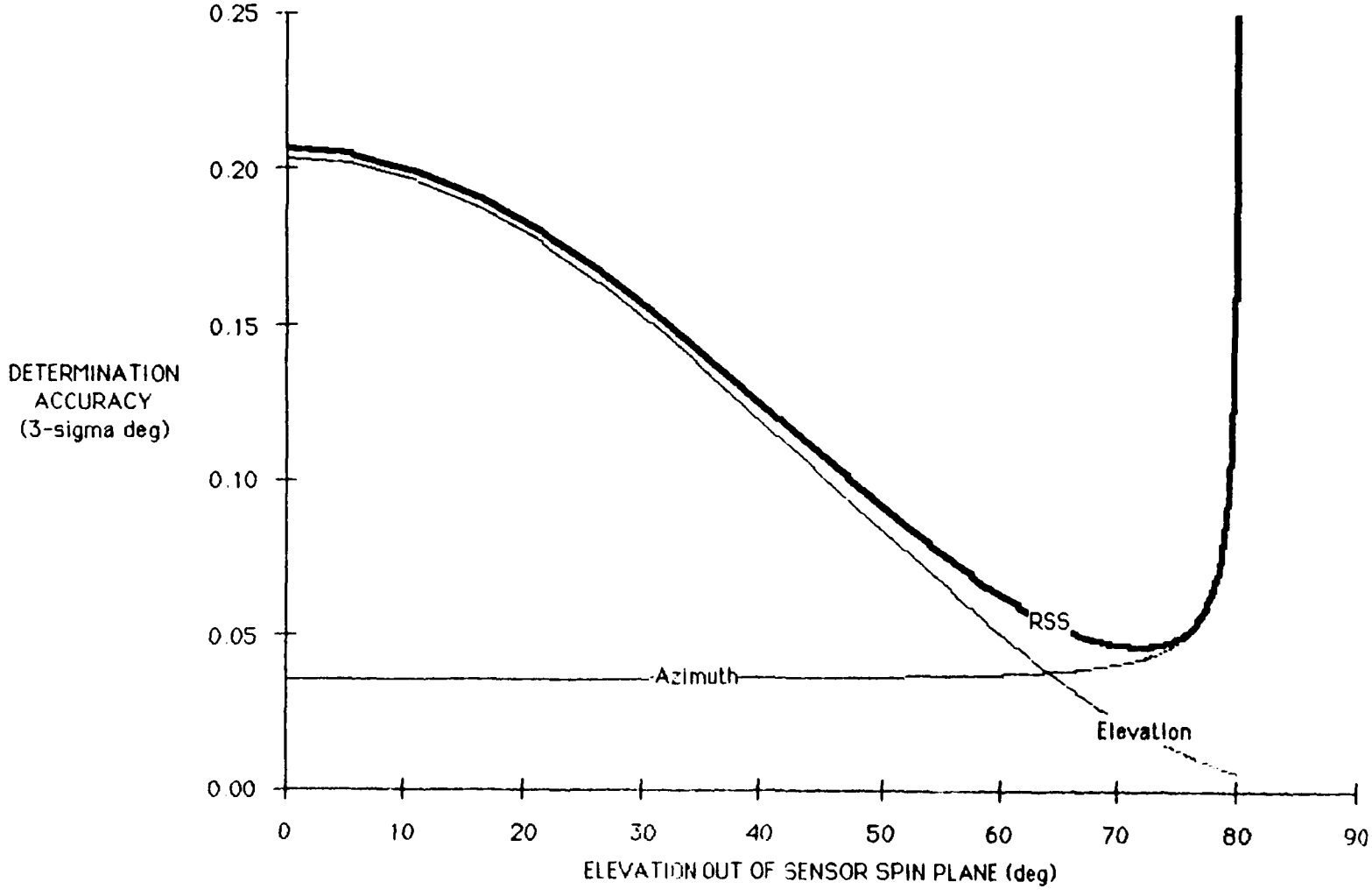

Figure 17. Moon attitude accuracy

Kalman filter algorithm with 1 second updates would place an excessive load on the on-board computer, which must process the data in real time. Secondly, the averaging algorithm can provide some error checking against noise outside the 3 . sigma level at low computational cost. The interval dt must not be too large, however, because the Kalman filter treats each datum as instantaneous, while in fact it represents an average over the preceding interval. During this time, the spacecraft moves and its attitude may change. We have selected dt = 25 seconds as a compromise update interval, but have done runs at 50 sec and 12.5 sec, with similar results. It would be desirable in future work to better evaluate on-board computing requirements for different update intervals.

We obtain the Sun and Moon position errors by averaging the results in Figs. 16 and 17 over solid angle, and dividing by 5 for our nominal 25 sec integration. The results are shown in Table 5.

Table 5. 3 Sigma Errors for Sun and Moon

	Azimuth (deg)	Elevation (deg)	RSS (deg)
Sun	0.001	0.006	0.006
Moon	0.001	0.03	0.03

Table 6 shows how to RSS the diverse errors to get the errors in the Earth Radius, Earth/Sun angle, and Earth/Moon angle.

Table 6. Final Interobject Angle Errors

	Resulting Angle		
Inputs	Earth Radius	Earth/Sun	Earth/Moon
Earth Radius	x		
Earth Attitude		x	x
Sun Attitude		x	
Moon Attitude			x
Error (deg, 3 sigma)			
Single ANS	0.0165	0.029	0.041
Dual ANS	0.0033	0.011	0.031

5.4 Attitude determination accuracies

Attitude determination algorithms for nadir-pointing satellites using Earth horizon and Sun (or Moon) direction data are given, for example, in Reference 4, Section 12.2. All required quantities are available from the ANS.

Attitude determination error using the technique covered above is principally a function of the accuracies of the Earth sensor, the Sun (or Moon) sensor, and their misalignments. Given the small errors contributed by the sensors themselves, the overall error is dominated by the misalignment of the sensor. Assuming a misalignment of 0.1 to 0.2 degrees, attitude determination will be maintained to this value in all cases, except when only sensing the Earth. In this case, yaw is not being determined.

6. Autonomous Navigation Algorithms

The orbiting of the spacecraft is described by dynamic equations. It is our purpose to determine the constants of motion (orbital elements) by fitting a calculated orbit to the real data. This is done, for example, for new comets or unidentified ballistic objects with only a few observations. There are two salient problems that prevent us from using classical methods based on a few observations in the current instance. One is that our sensors are less accurate than the desired precision in the orbital parameters, so that many observations must be averaged. The other is that there are forces on the craft that cause the elements to change with time. Solar and Lunar gravity perturbations, higher harmonics of the Earth gravity field, residual atmospheric drag, solar radiation pressure, and Earth IR and albedo radiation forces are potentially significant and can be modeled to various levels of accuracy. The hardest forces to model are radiation forces and atmospheric drag. Radiation forces are sensitive to attitude, and absorption and reflection coefficients. Atmospheric drag in LEO is sensitive to the variability of the exosphere.

Because of errors in the data, and unmodeled forces, the orbital equations cannot be fitted exactly to the data. Numerous techniques have been devised to obtain approximate fits. Most least squares methods have to be applied to fixed batches of data and are not readily adaptable to cases such as autonomous navigation where new data arrive continually or sporadically in various size batches. We desire a method that continues to make some use of the orbital history but that incorporates new data as they arrive. We consider two techniques (Ref. 4, pp. 459 - 469): Sequential Pseudo-inverse and Kalman Filter. Since the former is a special case of the latter we describe the Kalman Filter first.

6.1 Kalman Filter

The instantaneous state of the craft is described by a State Vector

$$XTRUE = (X,Y,Z,V_x,V_y,V_z). \tag{1}$$

In a more complex model, bias terms or attitude-related terms may be added to the state vector. The orbital equations to propagate XTRUE have the form

$$dXTRUE/dt = F * XTRUE + B. \tag{2}$$

F is a matrix expressing Newton's Second Law as applied in the Earth's gravity field, and B is a matrix of "other" forces such as radiation force. Air drag could go in F but would have additional dependence on the velocity that would have to be approximated to first order.

The observations are described by an observation vector y_{obs} which consists of a true part y plus an error component y_{err}, yielding

$$y_{obs}(i) = y(i) + y_{err}(i). \tag{3}$$

There are three components to y_{obs} and y: Earth-Radius (radius of the Earth image), Earth-Sun angle, and Earth-Moon angle. The error values are obtained from a Gaussian random number generator scaled by user-supplied one sigma RMS errors, *sigma1*, *sigma2*, and *sigma3*, respectively.

These observations must be compared with a vector g(i) of "model observations", i.e. observed values that would be *expected* on the basis of the estimated state vector XEST. The difference vector

$$rho(i) = y_{obs}(i) - g(i) \tag{4}$$

is then used to correct the estimated state vector. The algorithm for this correction process requires a few more matrices that must be defined. The matrix G(i,j) is defined as

$$G(i,j) = dg(i)/dXEST(j) \tag{5}$$

where the lower case letters "d" denote partial derivatives. Let R be the matrix

$$R = \text{diag}(sigma1^2, sigma2^2, sigma3^2), \tag{6}$$

and P the error covariance matrix,

$$P = E(XEST-XTRUE, XEST-XTRUE), \tag{7}$$

where E is the expectation operator (P is initialized using the assumed measurement errors). The process noise matrix Q is defined by

$$Q = \int D(t,s) * N(s) * V(s) * N^T(s) * D^T(t,s)ds \tag{8}$$

where

$$D(t,s) = \exp(F * (t-s)) \tag{9}$$

and F is defined in Eq.(2). The superscript T means transpose. The integration is over one time step. To explain the N and V terms we remark that for actual use on an assumed state vector XA, we must include a process noise term, viz:

$$dXA/dt = F * XA + B + N * n, \tag{10}$$

where n is zero mean white noise with covariance

$$E(n(t),n(t')) = V(t) * \text{delta}(t-t') \tag{11}$$

in which delta is the Dirac function and where N is an assumed matrix expressing how n affects the motion. In the present case, we take N to have zeros everywhere except three entries chosen so that n acts as a random force. V is user-supplied noise with dimensions of acceleration.

Process noise is essential when there are unmodeled forces. It causes the filter to have fading memory, so that it can accommodate long term drift. If it is chosen too large, the results will be noisy. If too small, the solution may show secular divergence or excess carryover of the effects of initial errors.

Finally, we define the crucial Kalman gain matrix as

$$K' = P * G^T[R + G * P * G^T]^{-1} \tag{12}$$

where the prime means that the quantity is corrected by applying the observations. The remaining Kalman correction equations are

$$XEST' = XEST + K * rho, \tag{13}$$

and

$$P' = [1 - K * G] * P. \tag{14}$$

In addition, one needs update equations to propagate P and XEST to the next time step. XEST is propagated by the same equation (2) as for XTRUE. (Remember, however, that since XEST is not perfectly accurate, errors in it will be propagated both *per se* and through wrong values in the coefficients F due to errors in the position. Furthermore, we sometimes insert *unmodeled forces* in (2) as applied to XTRUE but not to XEST). P is propagated by

$$P(t+dt) = P(t) + [F * P + P * F^T + Q]\, dt. \tag{15}$$

These equations complete the Kalman filter.

6.2 Pseudo-Inverse Filter

The Pseudo-Inverse is a special case where R is assumed to be zero and P a multiple of the identity matrix. (Ref. 4, p. 468) It is useful only when the observations are much more accurate than the state propagation process, and it fits only the most recent observations. This would cause a severe degradation at most times, because by integrating over many observations we are able to greatly enhance our accuracy. However, it could be used to initialize the Kalman filter after a maneuver or major change in input data.

7. Autonomous Navigation Simulator

The ANS simulation program follows a spacecraft in Earth orbit, modeling how it can track its own orbital motion using Earth, Sun, and Moon sensors. There are options to adjust the fraction of the orbit during which the various sensors are assumed to function. A Kalman filter estimates the current position and velocity from the simulated observations. Noise is present in the simulated observations and in the filter as "process noise." The program is designed primarily for LEO orbits but can be used at higher altitudes. (See Section 7.1 regarding the Sun-Moon angle and lunar parallax).

The program contains two main parts: an orbit propagator that simulates the spacecraft, orbit, attitude, and sensor data, and a sensor package/Kalman filter component that propagates the estimated state, simulates measurement of the appropriate angles and computes corrections to the estimated state parameters.

7.1 Earth, Sun, and Moon Models

The calculations are done in celestial coordinates. Analytic ephemerides of the Sun and Moon are used. The Sun and Moon sensors are blanked out (i.e., assumed not to return data) when the respective body is occulted by the Earth. The Earth sensor is assumed to work continuously. It measures the Earth radius and the Earth center location as expressed in the Sun-Earth (S/E) and Moon-Earth (M/E) angles. At present, the geocentric parallax of the Moon is ignored, so the Sun-Moon (M/S) angle varies only on the time scale of a month, and is useless for navigation. An on-board Kalman filter should include the correction for the geocentric parallax of the Moon but should probably not use the variation in the M/S angle over the orbit for navigation unless the altitude is of order one Earth radius or more, because the informational content would be low. Therefore, the present filter does not carry the M/S angle as a variable.

7.2 Sensor Model

The programs simulate the actual coverage of the Earth, Moon, and Sun. Simulator inputs include the mounting angle bias values, and the sensor noise levels. The Moon sensor will function poorly or not at all when the Moon is near "new" phase, i.e., not bright enough. An option is therefore included to delete Moon data near new Moon. In this option, the angle of "closeness" for losing the new Moon is user controlled with default 60 deg. The allowance of this option facilitates detailed realistic simulations, or more uniform parametric runs.

7.3 Simulator Inputs and Outputs

The inputs to the program along with their defaults are given in Tables 7 and 8.

Table 7. Simulator inputs

INPUT	DEFAULT	COMMENTS
A character string for the ASCII output file name		
Initial X, Y, and Z spacecraft coordinates (units of Earth radii)	0, -1.09, 0	300 NMi altitude
Initial X, Y, and Z velocities (LEO velocity units = 7906 m/s)	0.1663, 0.0, 0.9429	nearly circular orbit, i = 80°
Maximum estimated position error	$4.0 * 10^{-5}$	25 km
Estimated velocity error	$4.0 * 10^{-5}$	0.32 m/s
Initial Sun longitude offset (radians)	0.0	controls Sun independently of Julian day
Julian days since day 2447527	0.0	for Solar and Lunar ephemerides
Size of Moon sensor blanking disk (rad.)	0.0	simulates blockage or Sun interference
Kalman Fading Memory Factor (process noise)	0.0	also used 1-2 x 10^{-13}
Solar Radiation Force (fraction of Earth gravity force)	0.0	also used 10^{-6}
Earth Sensor Bias (deg)	0.0	adds to measured Earth radius
Sun Sensor Bias (deg)	0.0	adds to measured Sun-Earth angle
Moon Sensor Bias (deg)	0.0	adds to measured Earth-Moon angle

The sensor errors (one-sigma Gaussian distributed) depend on whether one or two ANS sensors are in use. For the two cases, the errors are as shown in Table 8.

Table 8. Sensor Errors

SENSOR	ONE ANS ERROR (deg, 1 sigma)	TWO ANS ERROR (deg, 1 sigma)
Earth sensor	0.0055	0.0011
Sun sensor	0.0097	0.0037
Moon sensor	0.0138	0.0105

The first filename is user-supplied and this file contains orbit-to-orbit details. The second filename contains 3 sigma navigation errors averaged over 3 orbits at a time. The navigation errors are given in several forms based on vector components along the following three unit vectors:

- Radial vector $\mathbf{r}^0$: along the radius from Earth center to craft.
- Out-of-Plane unit vector $\mathbf{w}^0$; in the direction of orbit normal.
- In-track Unit Vector $\mathbf{s}^0$: cross product $\mathbf{w}^0 \times \mathbf{r}^0$. The projection of navigation error on this vector is called the "in track error", but it is along the velocity only for circular orbits or at perigee and apogee for elliptical orbits.

The file contents are given in Tables 9 and 10. Sample plotted outputs follow in Figs. 19 to 22 (Section 8.1.1).

Table 9. Principal Outputs

Main Section (by columns):

1. One sigma navigation error (meters) = total displacement of estimated position from actual
2. One sigma radial navigation error (meters)
3. One sigma in-track navigation error (meters)
4. One sigma out-of-plane navigation error (meters)
5. One sigma velocity error (m/s)

6. Fraction of the orbital period in which the Sun was not sensed.

7. Fraction of the orbital period in which the Moon was not sensed.

8. Fraction of the orbital period during which at least one of the two objects (Sun or Moon) was visible.

9. Angle of Sun to orbit plane (deg); positive if in same sense as $\mathbf{w}^0$.

10. Angle of Moon to orbit plane (deg); same sign convention.

11. Angle between Sun and Moon vectors (deg).

12. End time of the orbit (hours).

Secondary Section (by columns):

1. 3 sigma navigation error (meters)

2. 3 sigma radial navigation error (meters)

3. 3 sigma in-track navigation error (meters)

4. 3 sigma out-of-plane navigation error (meters)

5. 3 sigma velocity error (m/s)

6. Fraction of the orbital period in which the Sun was not visible

7. Fraction of the orbital period in which the Moon was not visible

8. Fraction of the orbital period during which at least one of the two objects (Sun or Moon) was visible

A sample of a Main Output File is given in Table 10.

Table 10. Output for Fig. 20

```
The Output File Name is nom30.att
 Xtrue =  0.000E+000 -1.09E+000 0.000E+000 1.663E-001 0.000E+000 9.429E-001
 Inclination =    80.00 deg
 Xsigma =  4.000E-005 4.000E-005 4.000E-005 4.000E-005 4.000E-005 4.000E-005
 Xest =  -3.6304E-006 -1.0900E+000 -9.3294E-006 1.66292E-001 3.36341E-005 9.42862E-001
Default is Jan 0, 1989; Ephemerides are approximate
 Using Two Sensors
 RSS of Errors in the 3 Angles is: 1.11870E-002 (Not Including Biases)
Offset to the Initial Longitude of Sun= 0.000E+000
Enter Julian Days since 2447527 3.000E+001

Arc(rad) from "Sixp" blanking Moon 6.00E+000
Kalman fading memory factor = 0.00000E+000

Earth Radius Bias (deg)  = 0.000E+000
Earth Radius Sigma (deg) = 1.100E-003
Sun/Earth Angle Bias (deg)    = 0.000E+000
Sun/Earth Angle Sigma(deg)   = 3.700E-003
Moon/Earth Angle Bias (deg)   = 0.000E+000
Moon/Earth Angle Sigma  (deg) = 1.050E-002
Angle From Boresight to Velocity(deg) =     20.0

Time Step in seconds   = 2.5E+001
Frame Duration in sec   = 8.640E+004
Run Time Limit (simulated hours) = 2.400E+002

Ans averaged over    230  steps, i.e.  5.750E+003 seconds

The Sun and Moon angles below are to the Orbital Plane
```

Posn Error (meters)	Radial (meters)	In Track (meters)	OutOfPlane (meters)	Veloc (meters/sec)	S-ecl (frac)	M-ecl (frac)	OneVis (frac)	Sun angle	Moon angle	Mn/Sn angle	end-time (hours)
1.272E+002	1.228E+001	4.496E+001	1.130E+002	1.592E-001	0.343	1.000	0.657	-43	33	79	1.6
1.081E+002	3.467E+000	2.667E+001	1.019E+002	1.173E-001	0.343	1.000	0.657	-43	33	78	3.2
1.050E+002	3.439E+000	6.186E+001	8.076E+001	1.162E-001	0.343	1.000	0.657	-43	32	78	4.8
1.113E+002	1.926E+000	7.172E+001	7.945E+001	1.201E-001	0.339	1.000	0.661	-44	32	78	6.4
1.111E+002	1.467E+000	7.314E+001	7.876E+001	1.221E-001	0.339	1.000	0.661	-44	32	78	8.0
1.213E+002	1.517E+000	9.184E+001	7.371E+001	1.326E-001	0.343	1.000	0.657	-44	31	78	9.6
1.359E+002	2.063E+000	1.132E+002	6.922E+001	1.487E-001	0.339	1.000	0.661	-44	31	77	11.2
1.295E+002	1.857E+000	1.042E+002	7.050E+001	1.409E-001	0.339	1.000	0.661	-44	31	77	12.8
1.311E+002	1.226E+000	1.066E+002	7.063E+001	1.434E-001	0.339	1.000	0.661	-44	30	77	14.4
1.371E+002	1.125E+000	1.137E+002	7.049E+001	1.494E-001	0.339	1.000	0.661	-44	30	77	16.0
1.350E+002	1.413E+000	1.101E+002	7.173E+001	1.467E-001	0.339	1.000	0.661	-45	30	76	17.6
1.358E+002	1.775E+000	1.111E+002	7.193E+001	1.481E-001	0.335	1.000	0.665	-45	29	76	19.2
1.407E+002	1.753E+000	1.179E+002	7.077E+001	1.539E-001	0.335	1.000	0.665	-45	29	76	20.8
1.467E+002	1.641E+000	1.252E+002	7.003E+001	1.599E-001	0.339	1.000	0.661	-45	29	76	22.4
1.422E+002	1.351E+000	1.186E+002	7.200E+001	1.548E-001	0.335	1.000	0.665	-45	28	76	24.0

8. Navigation Performance

Let us open the discussion by setting a fiducial level of orbit determination accuracy based on simple triangulation and fixes. The orbit radius is of the order 1.09 Earth radii or 7000 km (3600 NMi). Typical three sigma sensor accuracies are of order 0.045 deg or 8×10^{-4} radian *after allowance* for repeated observation in our typical observing time of 25 sec. Multiplying by the orbit radius, we get a single-fix accuracy of about 6 km or 3 NMi prior to any filtering or long term averaging. The purpose of the Kalman filter is to allow the effective averaging of a large number of observations. Process noise must be introduced to keep the Kalman filter from diverging if there are unmodeled forces. If these forces are large, the noise parameter must be set large and the filter will track only coarsely.

When only the Earth and Sun are used, the data are invariant to rotation of the orbital plane around the Earth-Sun line. In this case the filter cannot correct orbital errors which are invariant under this rotation, such as error along track when the Sun is at the orbit pole, or periodic out-of-plane errors when the Sun is in the plane. As remarked in the introduction (Sect 2.2), however, this problem is not insoluble, because one may use position data for a moving reference body at different times in place of data on several reference bodies at one time to resolve such ambiguities. Alternatively, one may rely on the fact that orbit plane rotation is both slow and accurately predictable.

8.1 Results with No Biases or Unmodeled Forces

We shall first discuss the overall orbital accuracy in the simplest cases - with no sensor biases, or unmodeled forces. These are the results that would be anticipated after bias calibration and with unmodeled forces well below the level of the noise. There are four main subdivisions, according to whether there are 1 or 2 sensors and according to whether the Moon is in eclipse. Recall that near new Moon autonomous navigation will have to rely on Sun and Earth measurements only.

Within these four categories variations in navigation accuracy occur because of variations in the angle of the Sun and Moon out of the orbit plane and the relative phase of the Sun and Moon about orbit normal. Differing initial conditions are also important when the data do not provide good observations of all of the elements.

Fig. 18 shows the resulting accuracies for the four cases described above. On the ordinate we show the 3 sigma navigational error in meters. For the abscissa we wish to choose some measure of accuracy of the sensor package as a whole. For this purpose, we averaged the squared sensor errors for all three sensed angles, and took the square root. This is conservative in that the relatively large Moon sensor error is included even when the Moon is not available. We use this plot format in order to illustrate error dependency only on the sensor package or hardware, rather than on what objects are visible.

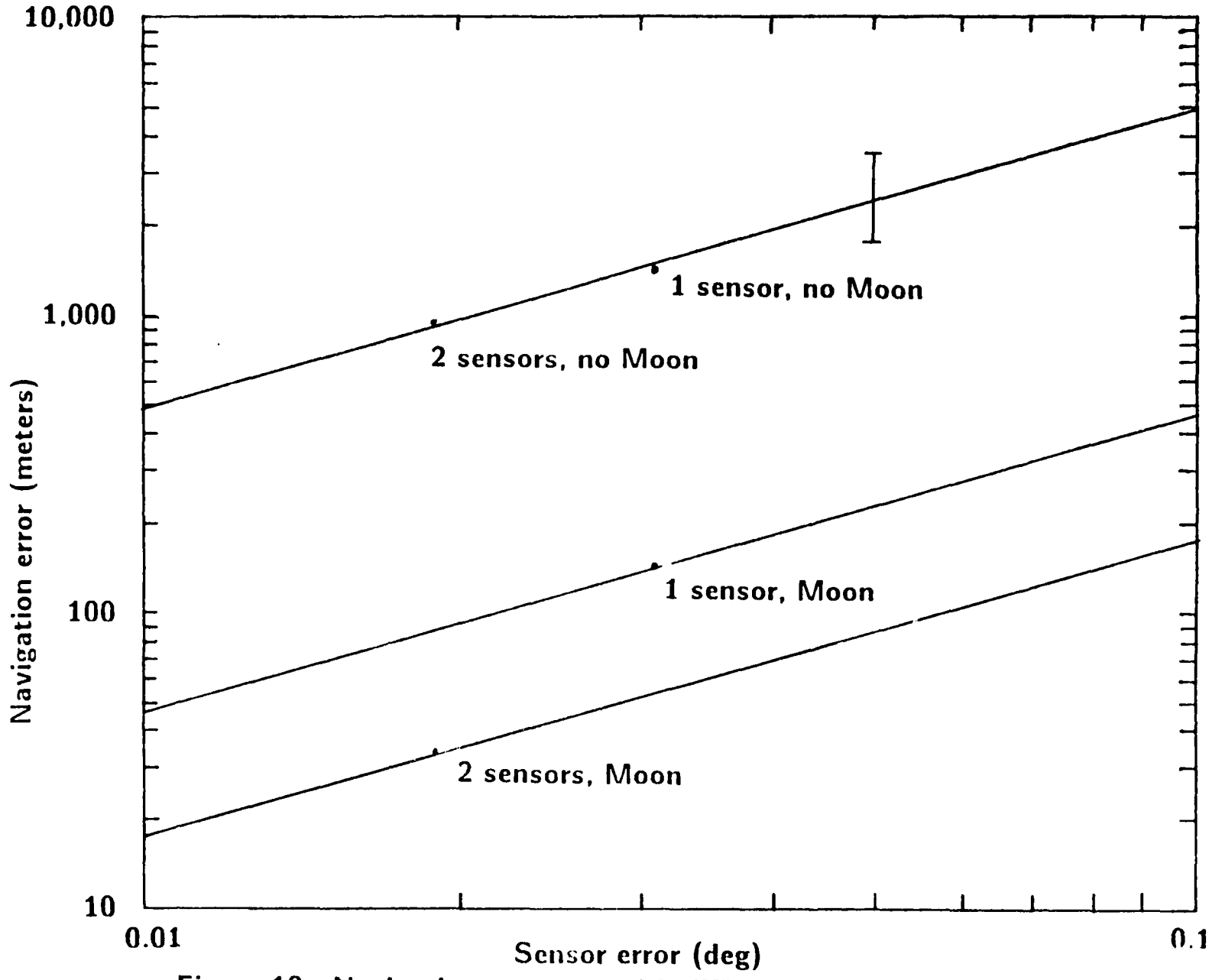

Figure 18. Navigation accuracy with different sensor coverage

The individual curves are averaged over several runs with different angles of the Sun (and/or Moon) to the orbital plane, different accuracies of the initial position and velocity estimates, and different values of the process noise figure. The labeled points indicate the actual numbers plotted. The variation from run to run for most cases is indicated. Linear dependence of navigation error on sensor error is expected and was verified by a number of runs at half, double, and four times the nominal sensor error values. The two "no-Moon" cases coincide within the width of the curves. This means that when only the Earth and Sun are visible, the additional sky coverage provided by the second sensor does not help, per se; only the improved angular resolution helps. Much of the error in these cases is persistent unidirectional in-track error or persistent oscillatory out-of-plane error due to ambiguity in rotation angle about the Earth/Sun line (see Sect. 2.2).

The most striking result of Fig. 17 is the increased accuracy when the Moon is visible. For these runs the Moon data were used even near new Moon. For comparison, extensive runs were also made going right through new Moon (with two sensors) where the Moon data *were* eliminated when the Moon was within 60 degrees of the Sun. These runs showed that good results were maintained through new Moon. The loss of accuracy during that period was negligible, due to the excellent Sun coverage. The lunar data then seem essential to have from time to time to reduce certain kinds of error, but are not needed all the time. This conclusion may require modification in the case of unmodeled forces.

In Sections 8.1.1 and 8.1.2 details of some runs will be given. First, however, consider the overall derived accuracy in comparison with single-fix accuracies. From Fig. 18 the mean 3 sigma accuracy varies from less than 100 meters (two sensors using Earth, Sun, and Moon) to 1.4 km (one sensor, Earth and Sun only). The improvement over a single fix (see beginning of Section 8) is thus a factor 4 to a factor 100. The factor 4 is a minimal improvement to be expected because we are averaging many observations. The factor 100 is justifiable because the filter can adjust the orbital elements using data acquired over many orbits.

The results we present next are for individual runs in sequences of frames of eight panels. Numbering these panels first down the left column, then down the right, the information is as follows:

Panel 1: *Plain curve* = Navigation error (displacement) in meters (RSS of all three components). *Curve interspersed with the letter "s"*: = theoretical 3 sigma error from trace of the space components of the P matrix [Sect. 5.1, Eq. (7)].

Panel 2: Radial component of displacement along $\mathbf{r}^0$ (m). This is always the smallest component because the sensor is accurate and the Earth is always visible.

Panel 3: In-track component of displacement, along $\mathbf{s}^0$ (m).

Panel 4: Out-of-plane component of displacement, along $\mathbf{w}^0$ (m).

Panel 5: RSS of the 3 components of velocity error (m/s).

Panel 6: Errors in the Sun/Earth angle (Monte Carlo and bias). When a stripe is shown, the Sun is eclipsed.

Panel 7: *Curve 1* = True Earth width. *Curve 2* = True Earth/Sun angle. (For non-circular orbits, curve 1 shows the appropriate oscillation.)

Panel 8: Earth/Moon angle. When the line is thick, the Moon is eclipsed.

The vertical scale in panels 1-5 is automatically adjusted. Figs. 19 to 22 show only a day's data, but most runs were extended to at least ten days. Runs were selected to show representative mean errors and to illustrate interesting dependencies. For example, one can see the navigation error get worse when reference objects are eclipsed. In longer runs one can even notice the in-plane error deteriorate most when an in-plane object is eclipsed or moves out-of-plane.

8.1.1 Results Using Earth and Sun Data

Figs. 19 and 20 show the beginnings of typical runs with no Moon available. In Fig. 19 a small amount of process noise was added and is evident in the in-track error. The Sun is only 28 deg from the orbital plane in this case, which should help control in-track error, but it happens to be eclipsed 63% of the time. These eclipses have, of course, the *same* periodicity as the orbit itself, which also accounts for the persistence of in-track error. With the Sun so close to the orbit plane, it is surprising that out-of-plane error is controlled so well. The tendency of eclipses to have the same period as the orbit hinders correction of the out-of-plane error as well. When the corrections to the orbit come repeatedly at the same phase of the out-of-plane oscillation, the error at *that* phase is over-corrected, leading to a ringing phenomenon.

In Fig. 20, the eclipses are shorter due mainly to better sky coverage. The Sun is 43 deg below the orbit plane. Without the process noise, the in-track error is quite persistent in sign. In general, adding process noise tends to break such locked-in errors but adds random variation in their stead. The beginning of the Main Output file for this run is shown in Table 10. Note that errors are 1 sigma in Table 10.

Our 80 deg inclination orbits precess slowly, and the Sun moves only a degree a day. This means that it may take a long time for the changing Sun angle to resolve the ambiguity of rotation about the Earth/Sun line. In a more realistic case unmodeled forces would probably harm the process. Thus it is best to count on at least occasional use of Moon data.

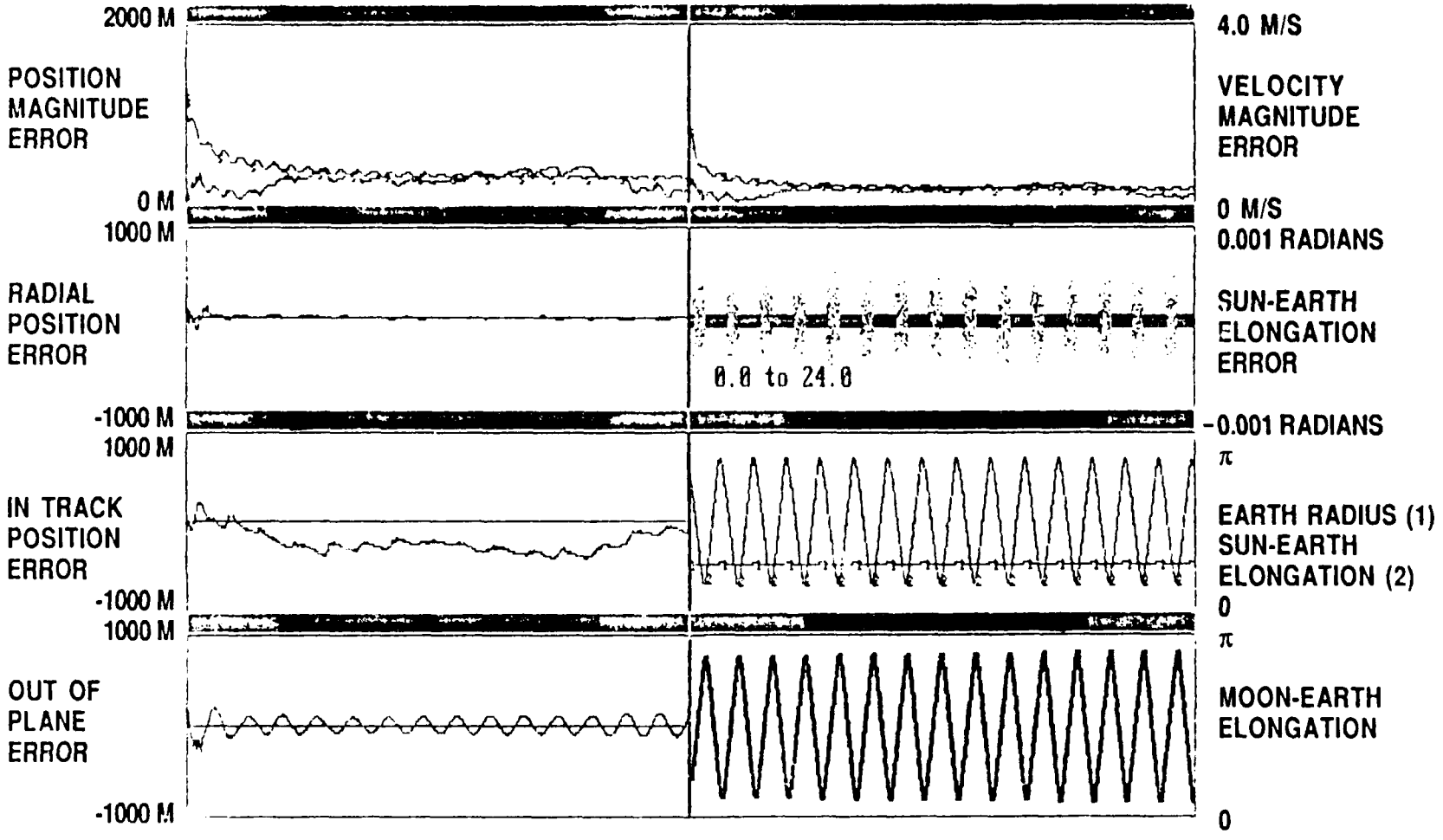

Figure 19. Outputs for 1 sensor and no Moon

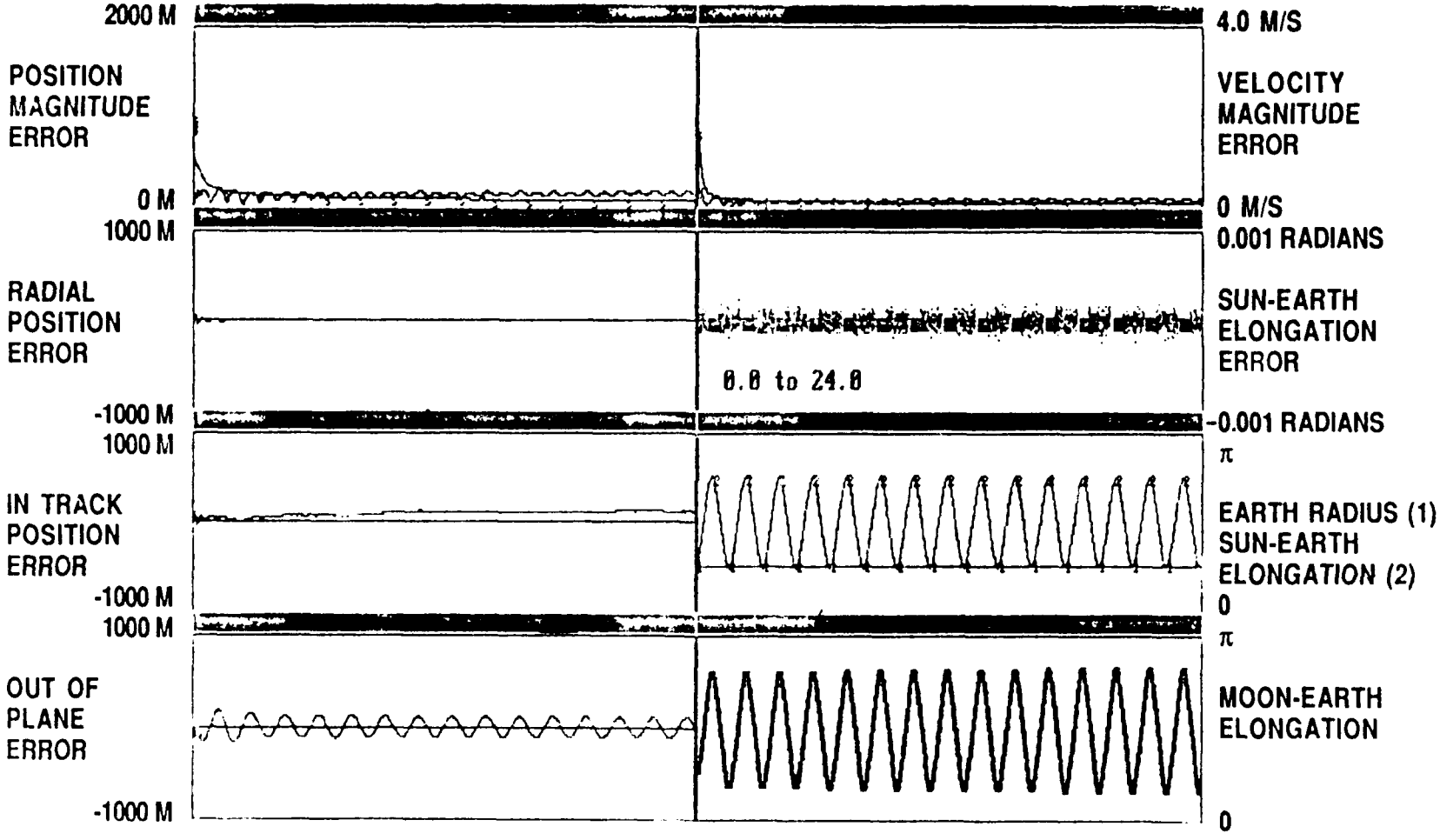

Figure 20. Outputs for 2 sensors and no Moon

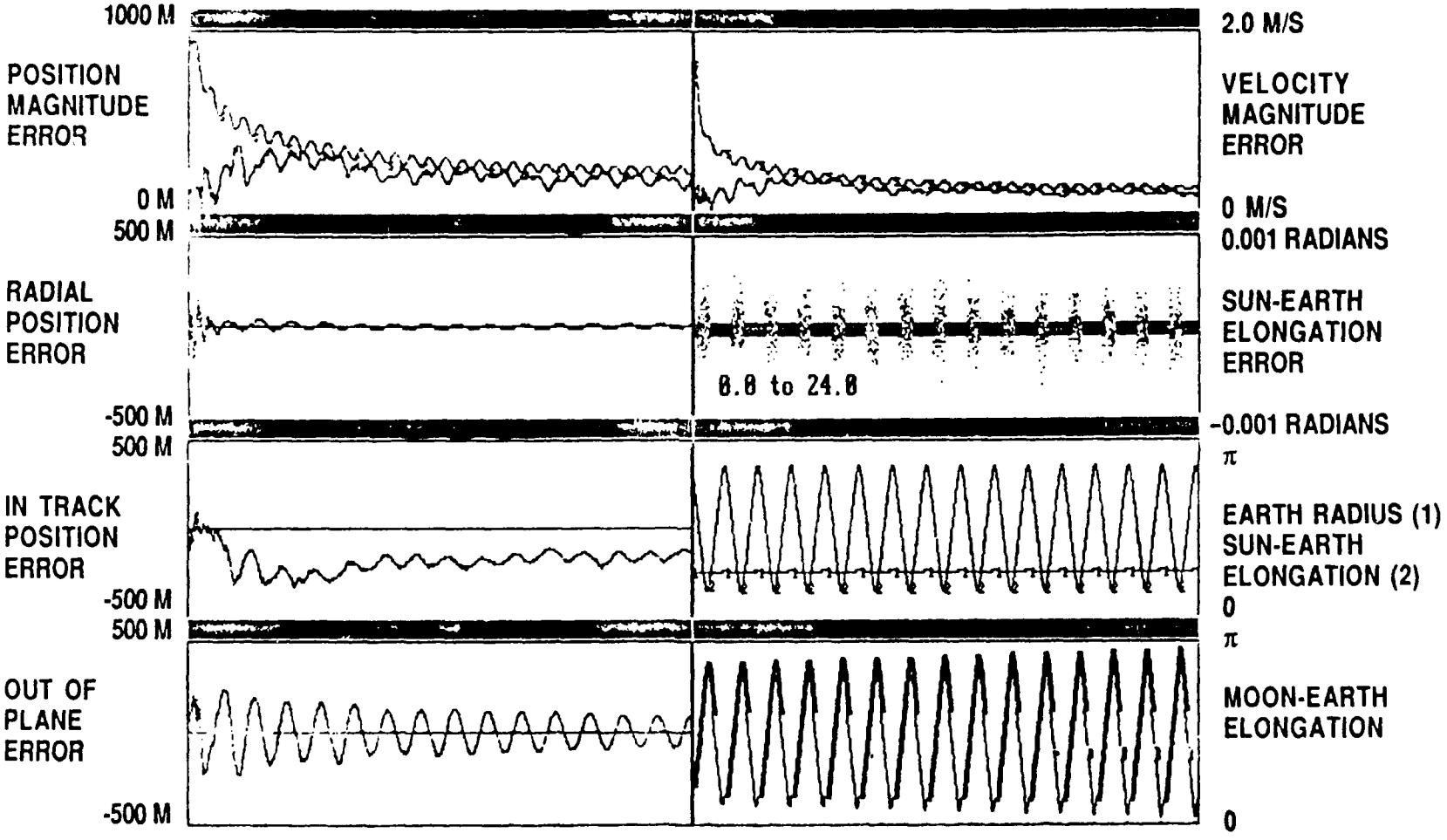

Figure 21. Outputs for 1 sensor with Moon

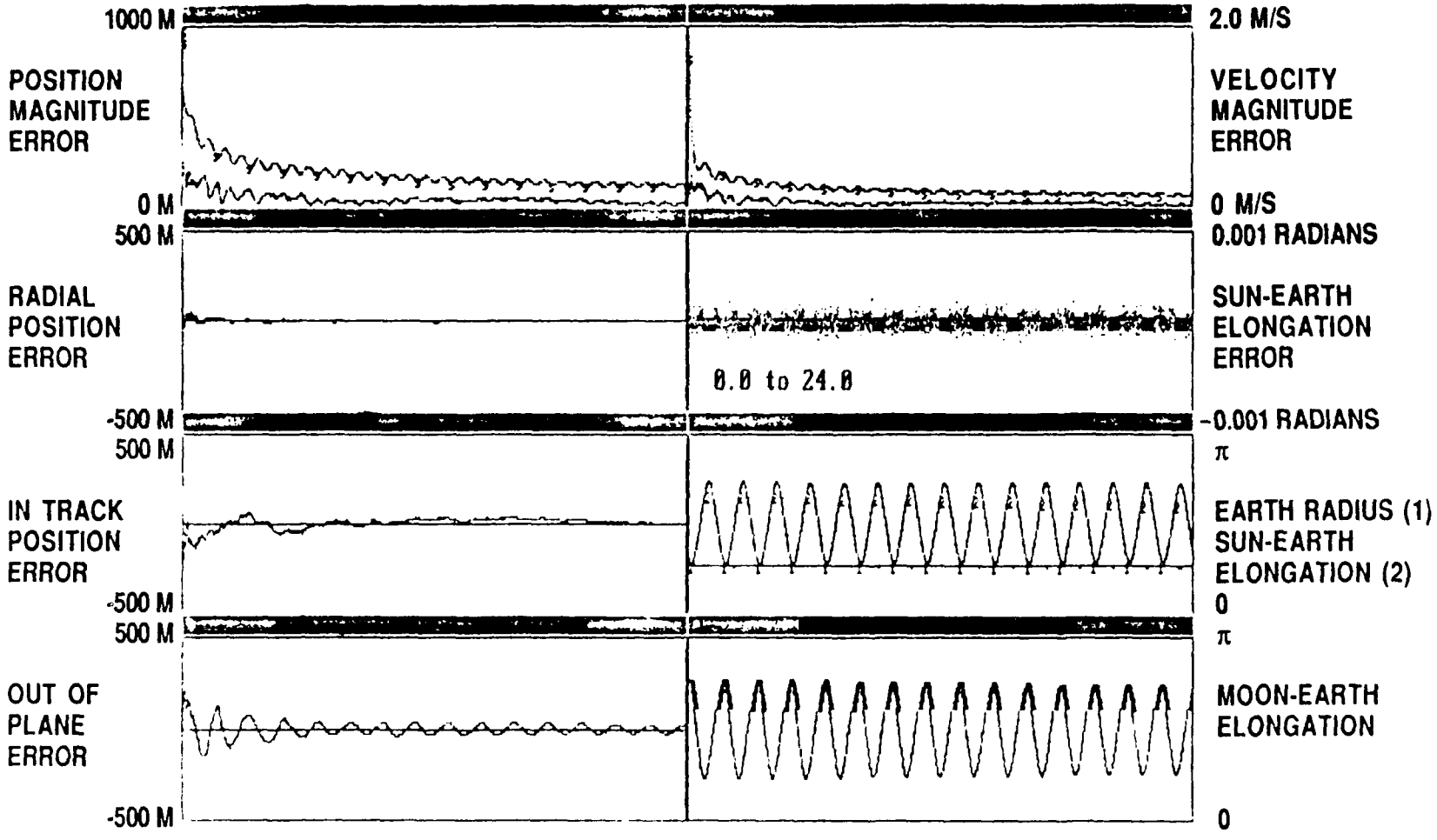

Figure 22. Outputs for 2 sensors with Moon

8.1.2. Results Using Earth, Sun, and Moon Data

The Moon offers two major advantages: i) it serves as a third reference point, and unless nearly collinear with the Sun, this resolves the rotation ambiguity; ii) it moves 12 degrees a day in the sky, so that periodicities in its visibility are not normally commensurate with orbital periodicities. This tends to reduce errors that are quite persistent in cases without the Moon. Figs. 21 and 22 show runs with the Moon visible some of the time. The vertical scales of panels 1-5 in these figures are half of those in Figs. 19 and 20. Notice how much improved the Moon coverage is with 2 sensors with which it is visible most of the time. Nevertheless, the presence of even sparse Moon data using 1 sensor is quite significant, bringing the navigational error down by a factor 10. Indeed, many runs gave 3 sigma navigational errors only of order 100 meters or less when using 1 sensor with Moon, but the variation from run to run was large. In the run shown (Fig. 21), the in-track and out-of-plane errors persisted for days. Only when using 2 sensors with Moon is the coverage sufficient to eliminate all geometrical ambiguities and to force the 3 sigma error consistently to less than 50 meters.

8.2 Results with Biases

As mentioned in section 5.1.2, biases or systematic errors can significantly degrade autonomous navigation performance and ordinarily will set the real performance limit. The residual bias errors, and therefore the autonomous navigation accuracy, will be determined by the level of in-flight calibration that is applied. This decision will be based on the accuracy versus the cost to achieve specific mission objectives.

For the present study we have assumed that on-orbit bias determination can be done to within an amount on the order of 0.01 deg. Typical results for one sensor with the Moon available are shown in Fig. 23. The scale of panels 1-5 in Figs. 23 and 24 is double that of Fig. 19. The biases were assumed to be 0.01 deg in Earth radius, -0.01 deg in Sun/Earth angle, and 0.0075 for the Moon/Earth angle. Notice the slope in each orbit's worth of Sun angle data (frame 6).

In these runs, the errors tended not to have much randomness nor dependence on the initial data. Thus it is meaningless to quote a 1 sigma or 3 sigma error and we give the navigation error, which is the RMS displacement over a typical orbit. The navigation error for these cases typically stabilized at 1 km, mostly out-of-plane.

Other cases were run with larger and smaller biases showing navigation errors proportional to the bias. Runs without process noise gave worse navigation errors. Similar runs with two sensors and the Moon available gave no improvement. This result is consistent with simple estimates based on scaling single-fix angular determinations by the major axis of the orbit.

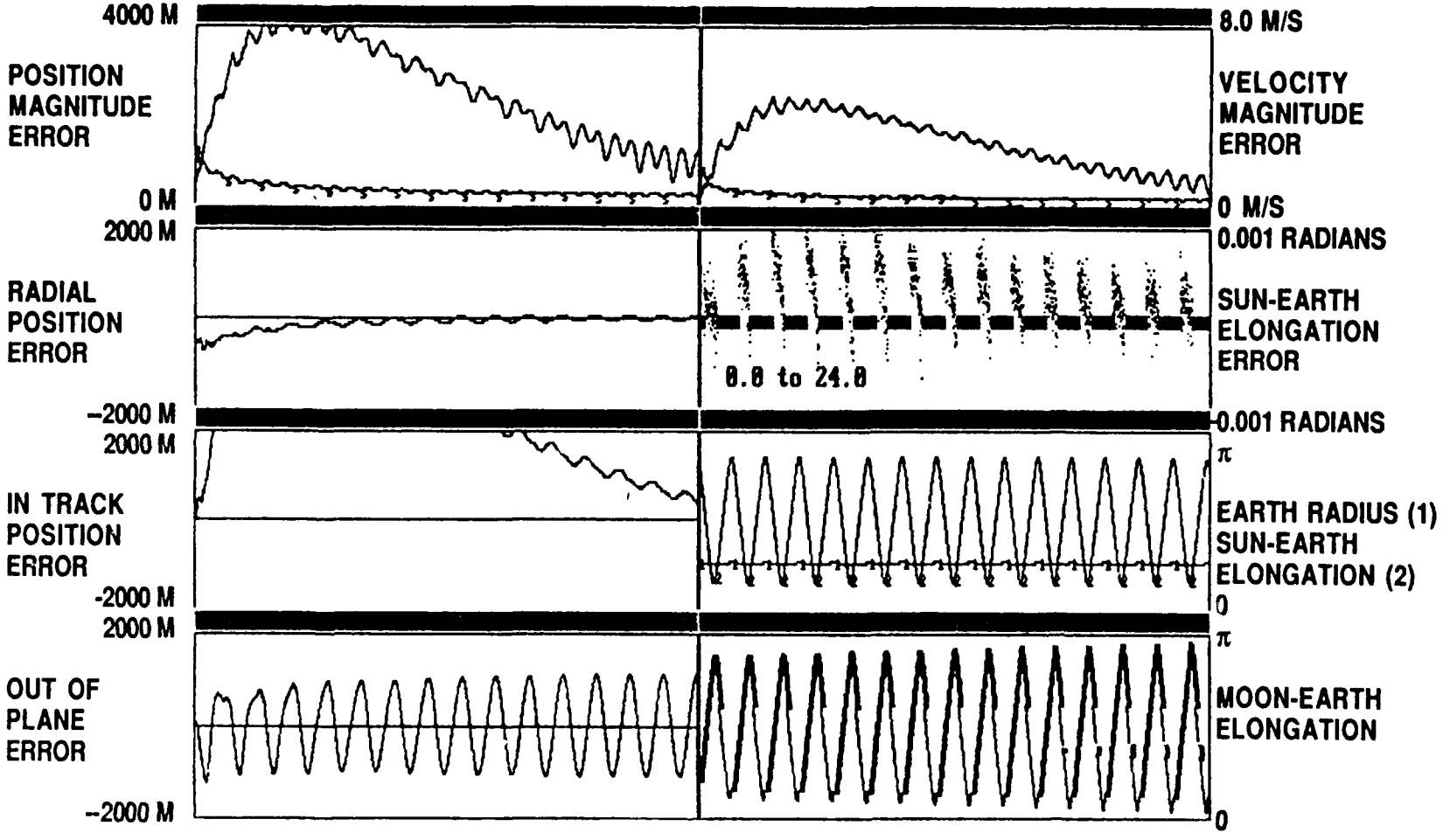

Figure 23. Outputs with sensor bias

8.3 Results with Unmodeled Forces

To test the ability of the Kalman filter to track in the presence of unmodeled forces, several runs were done with the force of solar radiation pressure present. An acceleration away from the Sun was added with a fixed value in sunlight and zero in eclipse. The force was only in the true orbit propagator, not in the Kalman filter propagator. A large force level was chosen to produce a perturbation sufficient to drive the filter to divergence when no process noise was included. Such a perturbation is readily visible in the graphics. As in Sect. 8.2, the navigation error is insensitive to initial conditions and random factors, so the actual navigation error rather than a 3-sigma level will be given. For the case shown in Fig. 24 the force was 10^{-6} of the Earth's surface gravity force. Several values of the process noise were tried and the best was selected. One sensor was used and the Moon was present. The navigation error stabilized at 250 meters. With two sensors the error was reduced to 150 meters--a result quite consistent with the linear dependence of navigation error on sensor error shown in Fig. 18. These are very encouraging results, considering the opportunity to model perturbative forces in detail.

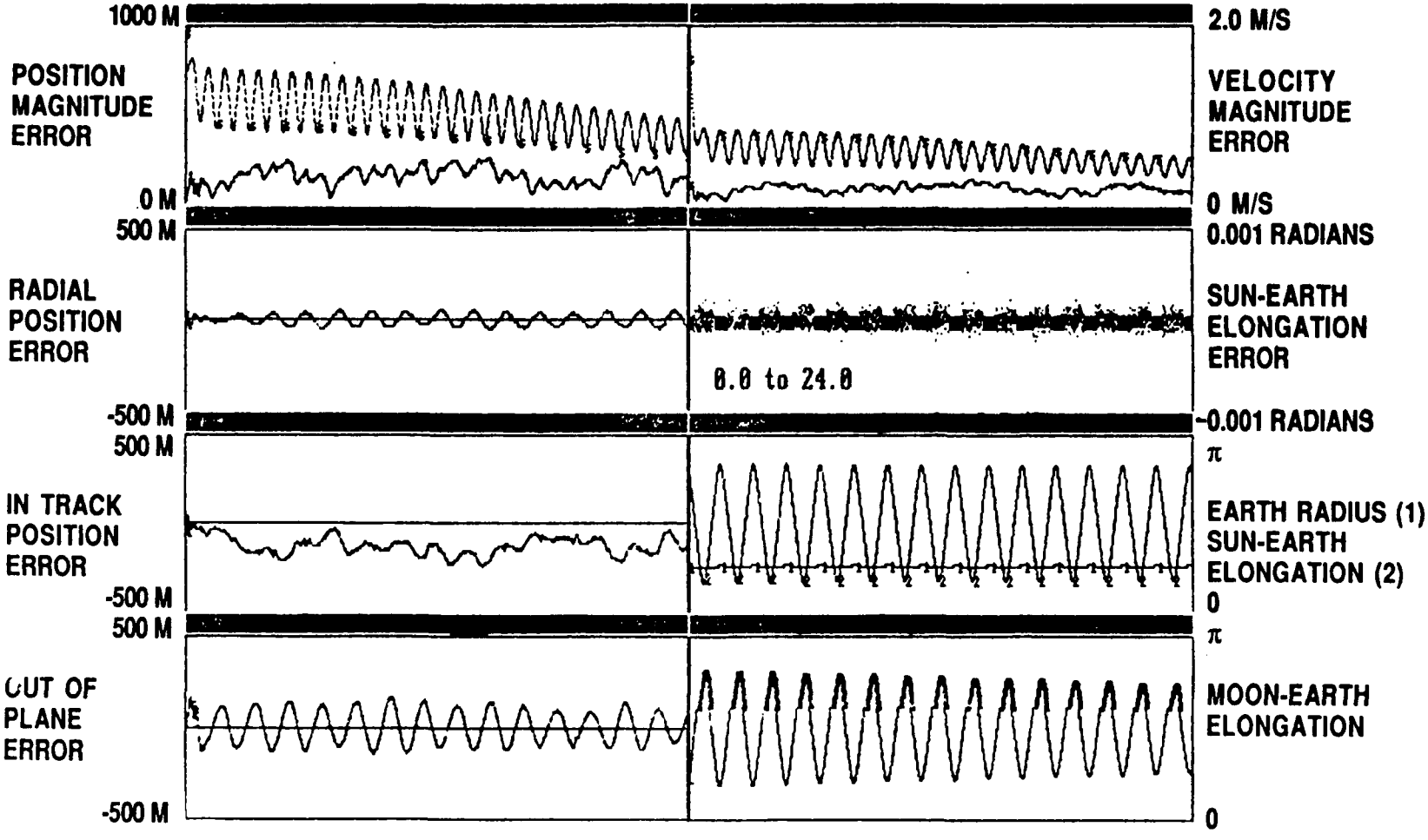

Figure 24. Outputs with unmodeled force

9. Flight System Development

Developments of the Autonomous Navigation System to produce a flight product will require the completion of the following tasks:

1. Sensor Configuration/Systems Engineering
2. Algorithm Development and Test
3. Sensor and Electronics Development and Test
4. Software Development and Test
5. System Integration and Qualification

Task 1 includes the work to tailor the ANS for a particular mission and to answer any remaining issues. The present study proposes an optical configuration and mounting orientation on the satellite designed for the general set of MSSP mission profiles. Enhanced performance can be achieved by adjusting each sensor set for the specific mission parameters of its satellite (i.e., its attitude, inclination, altitude, and spacecraft configuration). Further enhancements can gained by considering the additional studies covered in Sections 11.1 and 11.3. A few details that need to be resolved before proceeding include the level of analog hardware versus software computation and the Kalman update interval. Minimal cost and schedule for this Task 1 work has been included in the estimates for development of the sensor system since the majority of them, although desirable, are not essential for providing MSSP navigation.

Task 2, Algorithm Development and Test, will include additional simulation studies to determine robustness and navigation accuracy in the presence of more detailed satellite and orbital effects. These studies will determine those forces that can be ignored and those that must be modeled in the Kalman filter. As a result, significant algorithm enhancements (which will require additional modeling) may be required. A more complete description of this task is given in Section 11.2.

Task 3, Sensor and Electronics Development and Test, will be done following resolution of the sensor configuration issues in Task 1 and the analog electronics complexity issues in Task 2. An engineering model will be built, tested and then delta-qualified for its new Sun/Moon fan optics. This unit will also be used for the integration tests in Task 5.

Task 4, Software Development and Test, will be performed following the design of microprocessor algorithms in Tasks 1 and 2. A prototype of the flight software will be developed along with the flight data simulator and other simulations (i.e., satellite and orbit) necessary to test it. Following its qualification, a flight version of the software will be produced.

Task 5 will integrate the prototype hardware and the flight software and perform final verification tests for completion of the fully developed system. The tests will assure that the hardware and software interact together as individually simulated in Tasks 3 and 4 and that the set meets the requirements for flight qualification.

The result of the these 5 tasks will be to produce a fully qualified and tested sensor system consisting of protoflight hardware and flight software. Once developed, these AutoNav

systems could be provided in small quantities for a recurring cost of $25K above the cost of a standard Conical Earth Sensor, or a total hardware cost of only $275K.

An estimate of the schedule and budget required for development was made based on prior hardware and software experience and the predicted level of additional design required. It could be completed in 2.5 years by allowing 12 months for Task 1, 12 months for Tasks 3 and 4 performed concurrently, and then 6 months for Task 5. A modest level of schedule compression could be achieved by increasing manpower. They could be completed for a total non-recurring cost of approximately $1M, with $100K allocated to Tasks 1 and 2, $600K to Task 3, $250K to Task 4 and $100K to Task 5. These estimates, listed in Table 11, are for development of a non-optimal system to meet the requirements of MSSP (bracketed figures indicate work performed concurrently). Significant system capability enhancements can be made for the marginal increases in cost and schedule necessary to perform additional Task 1 work.

TABLE 11. Flight System Development Tasks

No.	Task	K$	Months
1&2	Configuration & Algorithm	100	12
3	Sensor & Electronics Devel	600	[11]
4	Software Devel	250	12
5	System Integration & Qual	100	6
	TOTAL	1050	30

10. Conclusions

A survey of satellite autonomous navigation capabilities shows that low cost systems using horizon sensors provide accuracies on the order of 500 meters to 8000 meters (see Fig. 1). Other types of systems provide better accuracy, but are either far more expensive or are not truly autonomous. The ANS uses low cost horizon sensor hardware, only slightly modified to provide the additional data necessary to perform navigation in a computationally straightforward manner. Single-look navigation accuracies of 6000 meters are predicted with this sensor, but in combination with a Kalman filter, accuracies as good as 100 meters can be achieved. The ANS accuracy, as plotted in Fig. 1, is shown to be an order of magnitude better than those of previous horizon scanner systems and it exceeds them all except those of the most expensive and sophisticated systems.

The ANS exceeded our performance expectations. Requiring minimal modifications to the attitude control hardware already flown on MSSP-type satellites, this system shows extreme promise for widespread application based on its high benefit for low cost.

11. Recommendations for Future Work

With the promising results from this preliminary study on low cost satellite autonomous navigation, follow-up work should be continued to verify the proposed concepts and to explore the limits of its capabilities, both in performance and applicability.

11.1 Sensor Design

11.1.1. Lunar Visibility

This study has shown (Sect. 8.1) that Moon visibility is important for accurate navigation; not only is the typical error an order of magnitude less when the Moon can be seen, but the variations with initial conditions are smaller. The limiting magnitude of the sensor with respect to the Moon should be assessed so that the time intervals of Moon visibility can be computed.

11.1.2 Error Budget; Calibrations

The internal error budget of the sensor package and electronics needs further evaluation to determine whether internal errors can be further reduced. Systematic sources of error need to be identified and procedures defined to calibrate for them. The accuracy of the calibration procedures then need laboratory testing in and modeling.

11.1.3 Microprocessor Sizing

In this study, the processing load has been adjusted to meet the capabilities of an existing Earth sensor flight-qualified CPU. The combined Earth/Sun/Moon sensor system will require additional signal processing as well as orbit propagation. Studies should be performed for trading off the level of orbit modeling desired, the amount of computation that can be off-loaded to analog electronics, and the impacts of increasing CPU capability.

By increasing the microcprocessor size and/or speed, it is possible to improve the performance. For example, the update rate of once per second assumed in the present study is due to the limitations of the microprocessor. The hardware can accommodate a much higher spin rate. Tradeoffs need to be considered in terms of increasing microprocessor capability including off-loading more of the work to hardwired (analog) electronics.

11.1.4 Scan Configuration

In this study, IR and Sun/Moon scan configuration (cone angles, fan angles, and spin axis orientation) were selected for the altitude and attitude

ranges of the MSSP satellites. In follow-up studies, these configurations need to be optimized for LEO, GEO, and transfer orbits. Full consideration of these issues requires assessment of coverage and accuracy (gain) considerations in conjunction with the performance of the Kalman filter. Optimizing coverage and then assessing accuracy may require more coverage of the sky in some areas (relative to the orbit) than others.

11.1.5 ANS Sensor Design for Spinning Spacecraft

The ANS was developed in this study for the three-axis stabilized, nadir pointing MSSP satellites. Even though a rotating design was incorporated to maximize coverage, inherent blockage by the satellite itself persists. Should a need arise for an autonomous navigation system on a spin-stabilized spacecraft, there is potential for gaining substantially better performance (no satellite blockage) and reducing cost (no need to rotate). An ANS for a spinning satellite should be developed and evaluated as it would represent the application of the proposed technology offering the greatest benefit versus cost.

11.2. Analysis

The next phase of the activity should result in a credible cost vs. performance model for the ANS including both orbit and attitude accuracy. Options should be provided based on sensor, dual sensors, or dual sensors plus gyros.

11.2.1 Additional Assessments Using the Current Simulator

The existing sensor/orbit simulator has been exercised sufficiently to determine its robustness and to obtain the results needed for the current project. Additional parametric studies of navigation accuracy should consider:

- Sun and Moon angle to the orbit plane
- Orbital inclination (which affects solar/lunar motion)
- Orbits other than MSSP--including GEO, GPS, transfer orbits, and low altitude/low inclination orbits.
- Initial accuracy of the orbit model
- Variations in Earth, Sun, and Moon coverage by the sensor
- Sensor mounting placement
- Optimization of the process noise level
- Impact of biases
- Impact of unmodeled forces
- Variations in update intervals
- Effect of maneuvers and their restart procedures

Recall that the apparent motion of the Sun and Moon during an orbit or over a few orbital periods can be useful in resolving singularities. There are obviously two key timescales over which solar or lunar motion is important: The orbital period and the period during which unmodeled forces or process noise cause loss of tracking - i.e. the "fading period" of the Kalman filter. The apparent motion of the Sun and Moon during an orbit or during the fading period will be affected by the altitude even more strongly than by the inclination, the latter effect being only due to nodal regression. In LEO we have found that the natural lunar motion helps but solar motion is so slow that it helps little. Going to higher orbits, one will find at first less solar

motion for most inclinations, due to the decreased regression of the node, and then eventually *more* solar motion per orbit due to the longer period. Thus there will be greatly increased possibilities for resolution of ambiguities/singularities through motion of the bright, easily sensed Sun at higher orbits; furthermore, the Moon will move more per orbit and both the Sun and Moon will be eclipsed far less. Runs under these conditions showed excellent performance.

11.2.2 Enhancements to the Orbit Propagator and measurement models

This report has addressed in detail the effects of sensor coverage, accuracy, bias calibration/elimination on navigational accuracy. The leading biases are:

- Atmospheric drag
- Lunisolar gravity perturbations
- Higher order gravitational harmonics
- Reaction forces due to attitude thrusters

Besides the sensor and bias quantities, the most important limiter of navigational accuracy is likely to be the process noise which is needed to allow the filter to follow the orbit with these unmodeled forces. Process noise passes through into navigational inaccuracy. The forces listed above need to be modeled and appropriate adjustment of the process noise level determined to allow fitting of residual errors (except that in the case of attitude thrusters, other procedures, such as re-initialization of the velocity might be needed).

In addition to the foregoing, there are unmodeled processes that contribute to the errors. The leading ones are:

- Ephemeris error, including on-board clock error
- Sensor biases, including relative bias if 2 ANS sensors are used
- Earth oblateness corrections
- Effect of spacecraft motion and attitude changes on the data.
- Detailed separate effects of sensor elevation and azimuth error .

For the next phase of system development all these issues must be addressed. In the case of the effect of attitude, it would be particularly desirable to devise and evaluate a method that keeps the attitude data out of the Kalman filter state data, because processing time would increase and convergence problems would likely arise in that case. In the case of detailed

sensor modeling, the simple RSS'ing of elevation and azimuth errors should be replaced with a model that used the attitude and mounting angle and the separate errors. Rather than averaging, a more realistic process of combining observations that are not simultaneous should be considered.

11.2.3 Other Enhancements

Several additional features should be added to the simulator and filter. On-orbit calibration and bias determination can significantly improve results. This process has traditionally been ground based. As an alternative, calibration and bias determination done on board can be explored. Detailed procedures will need to be worked out for the proposed sensor package.

The overall attitude determination accuracy available with the ANS sensor should also be evaluated. The effects of adding more sensors and of changing mounting angle combinations for multiple sensors should be included.

It is important to look at techniques for recovery after a maneuver or loss of data (e.g. from power interruption, intrusion of extraneous data from a natural or hostile source, etc.) The pseudo-inverse method is a likely candidate and could be worked into the present filter by introducing software switches. Another candidate is described in the appendix.

The inclusion of Sun/Earth/Moon rotation angle as an additional sensed item should be studied. This has the potential for improving accuracy with the existing data set.

11.3 Systems Engineering

It is desirable to evaluate the potential for using gyro data as a means of substantially upgrading AutoNav accuracy. By providing separate attitude data, gyros could assist in allowing for attitude changes during the data-taking interval or the Kalman filter update interval.

One should investigate further the potential applications and impact of the ANS on overall mission definition and design. For example, the orbital injection and initial accuracy of the ephemeris, the relationship of our independent ANS altitude information from the ephemeris, and the length and nature of the initial ground control phase will be issues. Failure mode operation and re-initialization of the attitude and orbit models in that case deserve study.

11.4 Flight System Development

To develop an actual flight system, one needs an engineering model of the ANS, a prototype of the flight software, and a flight data simulator. The engineering model would be developed following the resolution of the issues related to the

configuration of the IR cone angles and Sun/Moon fan angles, sensor rotation rate, and level of computation to be done by the analog electronics. The separation of elevation and azimuth errors and the modeling of attitude along with orbit will be the first essentials of the software. The means by which the individual data are averaged and sent to the Kalman filter must be decided, and the Kalman update interval would be determined by studying on-board processor cost vs. accuracy. The prototype flight software would be developed and tested in the flight data simulator with real-time and non-real-time modes.

12. REFERENCES

1. Chory, M.A., Hoffman, D.P., LeMay, J.L., "Satellite Autonomous Navigation - Status and History," Proceedings IEEE PLAN (Position, Location, and Navigation) Symposium, November, 1986

2. Chory, M.A., et al, "Autonomous Navigation -- Where We Are In 1984", Paper No. AIAA-84-1142-CP

3. Wertz, J.R., and Mullikin, T.L., "Reducing the Cost and Risk of Orbit Transfer," Paper No. AIAA-87-0172 presented to the AIAA 25th Aerospace Sciences Meeting, Jan. 12-15, 1987/ Reno, Nevada,

4. Wertz, J.R., ed. *Spacecraft Attitude Determination and Control*, D. Reidel Publishing Company, Dordrecht, Holland, 1978, 1980, 1984.

DISTRIBUTION LIST

addresses	number of copies
Steven W. Kabelis RADC/DCCR	6
RADC/DOVL GRIFFISS AFB NY 13441	1
RADC/DAP GRIFFISS AFB NY 13441	2
ADMINISTRATOR DEF TECH INF CTR ATTN: DTIC-DDA CAMERON STA BG 5 ALEXANDRIA VA 22304-6145	5
AFCSA/SAMI Attn: Miss Griffin 10363 Pentagon Wash DC 20330-5425	1
HQ USAF/SCTT Pentagon Wash DC 20330-5190	1
HQ AFSC/DLAE ANDREWS AFB DC 20334-5000	1
HQ AFSC/XRT Andrews AFB MD 20334-5000	1
HQ AFSC/XRK ANDREWS AFB MD 20334-500	1

HQ ESC/DCQR
Attn: Fred Lacwig
San Antonio TX 78243-5000 1

DTESA/RQEE
ATTN: LARRY G.MCMANLS
2501 YALE STREET SE
Airport Plaza, Suite 102
ALBUQUERQUE NM 87106 1

ASD-AFALC/AXP
WRIGHT-PATTERSON AFB OH 45433 1

ASD/AFALC/AXAE
Attn: W. H. Dungey
Wriight-Patterson AFE OH 45433-6533 1

ASD/ENACA
Wright-Patterson AFB OH 45433 1

AFIT/LDEE
BUILDING 640, AREA B
WRIGHT-PATTERSON AFB OH 45433-6583 1

AFWAL/MLTE
WRIGHT-PATTERSON AFB OH 45433 1

AFWAL/FIES/SURVIAC
WRIGHT-PATTERSON AFB OH 45433 1

AFHRL/OTS
WILLIAMS AFB AZ 85240-6457 1

AUL/LSE
MAXWELL AFB AL 36112-5564 1

HQ AFSPACECOM/XPYS
ATTN: DR. WILLIAM R. MATOUSH
PETERSON AFB CO 80914-5001 1

COMMAND CONTROL AND COMMUNICATIONS DIV
DEVELOPMENT CENTER
MARINE CORPS DEVELOPMENT & EDUCATION COMMAND
ATTN: CODE DICA
QUANTICO VA 22134-5080 2

COMMANDER
NAVAL OCEAN SYSTEMS CENTER
ATTN: TECHNICAL LIBRARY, CODE 9642B
SAN DIEGO CA 92152-5000 1

COMMANDER (CODE 3433)
ATTN: TECHNICAL LIBRARY
NAVAL WEAPONS CENTER
CHINA LAKE, CALIFORNIA 93555-6001 1

SUPERINTENDENT (CODE 1424)
NAVLA POST GRADUATE SCHOOL
MONTEREY CA 93943-5000 1

COMMANDING OFFICER
NAVAL RESEARCH LABORATORY
ATTN: CODE 2627
WASHINGTON DC 20375-5000 2

SPACE & NAVAL WARFARE SYSTEMS COMMAND
PMW 153-3DP
ATTN: R. SAVARESE
WASHINGTON DC 20363-5100 1

HQ ESC/CWPP
San Artonio TX 78243-5000 1

ESD/AVS 1
ATTN: ADV SYS DEV
HANSCOM AFB MA 01731-5000

ESD/ICP 1
HANSCOM AFB MA 01731-5000

ESD/AVSE 2
BLDG 1704
HANSCOM AFB MA 01731-5000

HQ ESD SYS-2 1
HANSCOM AFB MA 01731-5000

ESD/TCD-2 1
ATTN: CAPTAIN J. MEYER
HANSCOM AFB MA 01731-5000

Dr. Peter D. Noerdlinger 1
Rolling Hills Office Plaza
2601 Airport Drive, Suite 230
Torrance, CA. 90505

DARPA/ISTO 2
1400 Wilson Blvd.
Arlington Va. 22209

MISSION
of
Rome Air Development Center

RADC plans and executes research, development, test and selected acquisition programs in support of Command, Control, Communications and Intelligence (C^3I) activities. Technical and engineering support within areas of competence is provided to ESD Program Offices (POs) and other ESD elements to perform effective acquisition of C^3I systems. The areas of technical competence include communications, command and control, battle management, information processing, surveillance sensors, intelligence data collection and handling, solid state sciences, electromagnetics, and propagation, and electronic, maintainability, and compatibility.